Title
Photochemistry of ozone over the western Pacific from winter to spring

Journal
Journal of Geophysical Research D: Atmospheres, 109(23)

ISSN
0148-0227

Authors
Kondo, Y
Nakamura, K
Chen, G
et al.

Publication Date
2004-12-16

DOI
10.1029/2004JD004871

Photochemistry of ozone over the western Pacific from winter to spring

Y. Kondo,[1] K. Nakamura,[1] G. Chen,[2] N. Takegawa,[1] M. Koike,[3] Y. Miyazaki,[1] K. Kita,[4] J. Crawford,[2] M. Ko,[2] D. R. Blake,[5] S. Kawakami,[6] T. Shirai,[6] B. Liley,[7] Y. Wang,[8] and T. Ogawa[6]

Received 6 April 2004; revised 2 July 2004; accepted 20 July 2004; published 14 October 2004.

[1] Aircraft measurements of ozone (O_3) and its precursors, including NO, CO, H_2O, and nonmethane hydrocarbons (NMHCs), were made over the western Pacific in the 20°–45°N latitude range in January and April–May 2002 during the Pacific Exploration of Asian Continental Emission (PEACE)-A and B campaigns. These measurements have provided data sets that, in combination with Transport and Chemical Evolution over the Pacific (TRACE-P) data taken in March 2001, enable studies of O_3 photochemistry from winter to late spring. A photochemical box model is used to calculate ozone formation ($F(O_3)$) and destruction ($D(O_3)$) rates constrained by the observed species concentrations. The values of $F(O_3)$ and $D(O_3)$ are controlled directly by NO, $J(O^1D)$ (O_3 photolysis frequency), H_2O, OH, and HO_2. Changes in HO_2 concentration cause corresponding changes in both $F(O_3)$ and $D(O_3)$, leading to their coupling. Concentrations of these species, which are strongly influenced by photochemistry and transport from the Asian continent, underwent large seasonal variations. In the boundary layer (0–3 km), NO was much higher in January than in April–May, because of stronger winds, lower convective activities, and lower oxidation rates by OH in winter. The net O_3 formation rate, given by $P(O_3) = F(O_3) - D(O_3)$, was largely positive in the boundary layer at 30°–45°N (1.5 − 4 ppbv d^{-1}) in January, mainly because of high NO and low H_2O values. Net O_3 formation continued from January to the end of March, demonstrating that the western Pacific is an important O_3 source region during this season. Net O_3 formation nearly ceased by late April/May because of the decrease in NO and the increase in H_2O. In the latitude range of 20°–30°N, $P(O_3)$ in the boundary layer was positive in January and turned negative by March. The earlier transition was mainly due to lower NO and higher H_2O concentrations, combined with weaker transport and higher temperatures than those at 30°–45°N. The upper troposphere (6–12 km) has been shown to be a region of net O_3 formation throughout most of the year because of high NO and low H_2O. The present study illustrates that a decrease in the net O_3 formation rate at 20°–45°N latitude from winter to late spring is explained systematically by the increases in $J(O^1D)$, H_2O, OH, and HO_2 (primarily due to increases in temperature and solar radiation) and the decrease in NO (primarily due to decrease in transport from the Asian continent). Differences in the seasonal variation of O_3 photochemistry observed over the North American continent are interpreted in terms of the differences in factors controlling O_3 formation and destruction. *INDEX TERMS:* 0365 Atmospheric Composition and Structure: Troposphere—composition and chemistry; 0368 Atmospheric Composition and Structure: Troposphere—constituent transport and chemistry; 0345 Atmospheric Composition and Structure: Pollution—urban and regional (0305); 0322 Atmospheric Composition and Structure: Constituent sources and sinks; *KEYWORDS:* ozone, troposphere, western Pacific

Citation: Kondo, Y., et al. (2004), Photochemistry of ozone over the western Pacific from winter to spring, *J. Geophys. Res.*, *109*, D23S02, doi:10.1029/2004JD004871.

[1]Research Center for Advanced Science and Technology, University of Tokyo, Tokyo, Japan.
[2]NASA Langley Research Center, Hampton, Virginia, USA.
[3]Department of Earth and Planetary Science, Graduate School of Science, University of Tokyo, Tokyo, Japan.
[4]Department of Environmental Science, Graduate School of Science, Ibaraki University, Mito, Japan.
[5]Department of Chemistry, University of California, Irvine, California, USA.
[6]Earth Observation Research and Application Center, Japan Aerospace Exploration Agency, Tokyo, Japan.
[7]National Institute of Water and Atmospheric Research, Lauder, New Zealand.
[8]School of Earth and Atmospheric Sciences, Georgia Institute of Technology, Atlanta, Georgia, USA.

0148-0227/04/2004JD004871

1. Introduction

[2] Ozone (O_3) in the troposphere is a principal precursor of the hydroxyl radical (OH) and nitrate radical (NO_3), which control the oxidizing capacity of the atmosphere [e.g., *Logan et al.*, 1981; *Thompson*, 1992]. Ozone is also a major pollutant, because it has adverse effects on human health and plants at high concentrations. Ozone is chemically produced in the troposphere by OH-initiated oxidation of CO, CH_4, and nonmethane hydrocarbons (NMHCs). NO_x(= NO + NO_2) acts as a key catalyst in these cycles. East Asia is a region where rapidly growing industrial activities are causing large increases in the emissions of these O_3 precursors. Specifically, emissions of NO_x in Asia are estimated to have increased by a factor of 3 between 1975 and 1998 [*Akimoto*, 2003]. Another study showed a nearly 40% increase from 1990 to 2002 [*Streets et al.*, 2003]. Emissions of these pollutants from the Asian continent can significantly impact the distributions of O_3 over the western Pacific, downwind of the Asian continent.

[3] One of the important features of tropospheric O_3 is that its mixing ratios reach maximum values in late spring in many regions of the northern midlatitudes, including over the western Pacific [*Logan*, 1985, 1999]. The budget of seasonal variations in O_3 has been investigated with 3-D models [e.g., *Wang et al.*, 1998b; *Yienger et al.*, 1999]. However, estimates of the O_3 budget will remain uncertain unless predicted concentrations of related trace gases are validated by observations of key chemical species. A lack of seasonally and geographically resolved stratospheric O_3 flux measurements represents another major uncertainty. Budgets of reactive nitrogen and O_3 over the North American continent were studied by the Tropospheric Ozone Production about the Spring Equinox (TOPSE) aircraft campaign made at middle and high latitudes in winter-spring [*Atlas et al.*, 2003]. Photochemical O_3 processes in these regions were studied with a photochemical box model [*Wang et al.*, 2003; *Cantrell et al.*, 2003b] and with 3-D models [*Emmons et al.*, 2003]. Budgets of O_3 over the western Pacific from early to middle spring were estimated with photochemical box model calculations using the data set obtained from February to April 2001 during the NASA Transport and Chemical Evolution over the Pacific (TRACE-P) campaign and the Pacific Exploratory Mission (PEM)-W-B [*Davis et al.*, 2003]. However, comprehensive measurements in winter and late spring are still very limited, although some data were obtained during the Biomass Burning and Lightning Experiment (BIBLE)-T campaign of the Japan Aerospace Exploration Agency (JAXA) in late April 1998 [*Miyazaki et al.*, 2002]. In order to improve our understanding of O_3 chemistry during these periods, the aircraft measurement campaigns Pacific Exploration of Asian Continental Emission (PEACE)-A and B were conducted in January and April–May 2002, respectively, within the framework of the atmospheric chemistry project of the Earth Observation Research Center (EORC) of JAXA. We have investigated the seasonal variation of the formation and destruction processes of HO_x (OH + HO_2) and O_3 in the region of 20°–45°N latitude from winter to late spring using the same photochemical box model as used by *Davis et al.* [2003]. The data sets obtained by the PEACE and TRACE-P campaigns have been used as input parameters to constrain this model. Major factors controlling the budgets of O_3 and HO_x in different seasons have been quantified by these calculations.

2. Aircraft Measurements

[4] In situ chemical data obtained on board the G-II aircraft were used for this study. The measured quantities include O_3, CO, NMHCs, NO, total reactive nitrogen (NO_y), H_2O, and the photolysis frequency of NO_2 ($J(NO_2)$). The instruments used for the PEACE aircraft measurements are the same as those used for BIBLE-B campaigns [*Kondo et al.*, 2002], with an addition of an SO_2 instrument. The techniques, uncertainties (accuracy and precision), and time resolutions of these measurements are summarized by *Parrish et al.* [2004, Table 1]. In addition, the $J(NO_2)$ instrument was calibrated at Lauder, New Zealand (45°S), using a National Institute of Water and Atmospheric Research (NIWA) spectroradiometer along with a radiative transfer model to convert irradiances from that instrument to actinic fluxes [*McKenzie et al.*, 2003]. All necessary inputs to the model were available, and the instrumentation, analysis methods, and radiative transfer model have all been verified previously [*Bais et al.*, 2001; *McKenzie et al.*, 2002; *Cantrell et al.*, 2003a]. On the basis of these calibrations, we estimate that the $J(NO_2)$ measurement during the PEACE campaigns has an uncertainty of 7%. The O_3, CO, NO, NO_y, H_2O, and $J(NO_2)$ data were then averaged using a common time base with an interval of 1 min. The NMHC data, which were obtained every 5 min on average, were interpolated to produce 1-min data, when changes in CO and altitude were small. The G-II was based in Nagoya (35.3°N, 136.9°E) and Kagoshima (31.6°N, 130.5°E) during PEACE-A. Thirteen flights were conducted during the period between 6 and 23 January 2002 as shown by *Parrish et al.*[2004, Table 3a]. The flight tracks are shown in Figure 1. During PEACE-B, the G-II was based in Nagoya, and 12 flights were conducted during the period between 21 April and 16 May 2002 [*Parrish et al.*, 2004, Figure 1 and Table 3b]. The altitude of airborne sampling ranged between 0.1 and 13 km. Flights made during PEACE-A covered the latitudes between 22°N and 42°N. Flights during PEACE-B covered similar latitudes. However, because the quantity of data south of 30°N was much smaller than during PEACE-A, the statistical analysis of the PEACE-B data was limited to the latitude range of 30°–42°N.

[5] During TRACE-P, concentrations of O_3 and its precursors were measured over the western Pacific on board the P-3B and DC-8 aircraft in February–April 2001 [*Jacob et al.*, 2003]. These data were also used for the present analysis. The TRACE-P measurements covered the latitude range between 15°–45°N over the western Pacific, as shown in Figure 1.

3. Photochemistry of O_3 and Box Model

[6] For the present study, a time-dependent photochemical box model [*Crawford et al.*, 1997; *Davis et al.*, 2003; G. Chen et al., A diagnostic analysis of winter/spring ozone budget based on ozonesonde and airborne observations from PEACE A/B and TRACE-P, submitted to *Journal of Geophysical Research*, 2004, hereinafter referred to as Chen et al., submitted manuscript, 2004] was used in order to estimate radical concentrations, including NO_2, and to

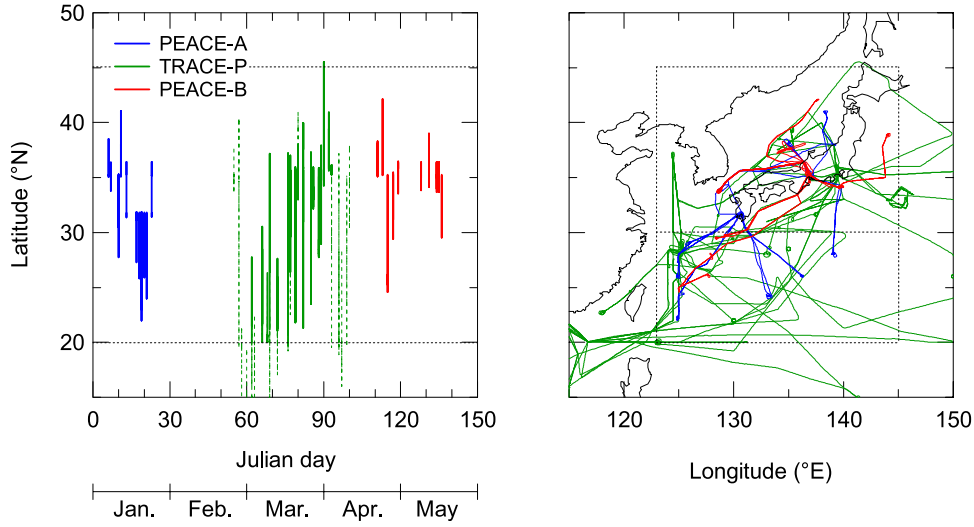

Figure 1. Latitudes and periods covered by the PEACE-A, TRACE-P, and PEACE-B campaigns and their flight tracks.

quantitatively assess the photochemical impact on O_3. This box model was applied to the analysis of O_3 photochemistry using the data sets obtained during the NASA missions PEM-W-A, PEM-W-B, and TRACE-P. The key reactions for O_3 photochemistry considered in this model are discussed by *Crawford et al.* [1997] and are listed in Table 1. HO_x is initially formed by the photolysis of O_3 at wavelengths of 290–320 nm (reaction (R1)). The rate of HO_x formation is expressed as

$$F(HO_x) = 2k_1 k_{3a}[O_3][H_2O]/(k_{3b}[M] + k_{3a}[H_2O]) \approx 2k_1 k_{3a}[O_3][H_2O]/k_{3b}[M], \quad (1)$$

where [ ] denotes the number density of the indicated species, k_i is the reaction rate coefficient for reaction R_i, and $k_1 = J(O^1D)$ is the photolysis frequency of O_3. This equation shows that the key parameters driving the HO_x primary production are solar ultraviolet (UV) radiation, O_3, and H_2O. At the same time, formation of HO_x results in O_3 loss. Net photochemical loss of HO_x occurs through reactions (R9) and (R12). Under high-NO_x conditions, reaction (R12) dominates as a sink of HO_x; for low NO_x, reaction (R9) does. NO also controls the partitioning between OH and HO_2 through reaction (R4). Oxidation of CO, CH_4, and NMHCs by OH leads to the formation of peroxy radicals HO_2, CH_3O_2, and RO_2 (R = C_2H_5 and higher organic groupings). These radicals react with NO, leading to catalytic O_3 formation (reactions (R4), (R5), (R6), (R10), (R11), and (R2)). Photochemical destruction of O_3 occurs through reactions (R1) + (R3a), (R7), and (R8), with reaction (R3a) being dominant for the lowest part of the troposphere. The photochemical formation ($F(O_3)$), destruction ($D(O_3)$), and net formation ($P(O_3)$) rates are expressed as

$$F(O_3) = (k_4[HO_2] + k_5[CH_3O_2] + k_6[RO_2])[NO], \quad (2)$$

$$D(O_3) = k_{3a}[O(^1D)][H_2O] + (k_7[OH] + k_8[HO_2])[O_3] + k_{10}[NO][O_3] \times k_{12}[NO_2][OH]/(k_{11}[NO_2] + k_{12}[NO_2][OH]), \quad (3)$$

$$P(O_3) = F(O_3) - D(O_3). \quad (4)$$

The last term in equation (3) becomes significant only at NO_x levels exceeding ≈500 parts per trillion by volume (pptv). The $F(O_3)$ and $D(O_3)$ values increase linearly with [NO] and [O_3], respectively (equations (2) and (3)), when concentrations of other species are unchanged.

[7] The time-dependent box model was run using the observed values of NO, CO, O_3, H_2O, NMHCs, $J(NO_2)$, temperature, and pressure as input parameters. The other photolysis frequencies were initially calculated with the NCAR Tropospheric Ultraviolet Visible (TUV) radiative transfer model with a DISORT four-stream implementation for clear-sky conditions. The observations of $J(NO_2)$ relative to calculated clear-sky values were used to scale these values for the cloudy conditions encountered during the sampling.

[8] Model integration was continued until the model outputs reached diurnal stationary state. For most of the present analysis, diurnally averaged values of radicals, $F(O_3)$, $D(O_3)$, and $P(O_3)$ were used. *Olson et al.* [2004] showed good model agreement with the observed total peroxy radical concentrations (with a median bias of 23%). Similarly, calculated NO_2 concentrations at 0–7 km agreed

Table 1. Key Reactions in O_3 Photochemistry

Reaction No.	Reaction
(R1)	$O_3 + h\nu \rightarrow O_2 + O(^1D)$
(R2)	$O(^3P) + O_2 + M \rightarrow O_3 + M$
(R3a)	$O(^1D) + H_2O \rightarrow 2OH$
(R3b)	$O(^1D) + M \rightarrow O(^3P) + M$
(R4)	$HO_2 + NO \rightarrow NO_2 + OH$
(R5)	$CH_3O_2 + NO \rightarrow NO_2 + CH_3O$
(R6)	$RO_2 + NO \rightarrow NO_2 + RO$
(R7)	$O_3 + OH \rightarrow HO_2 + O_2$
(R8)	$O_3 + HO_2 \rightarrow 2O_2 + OH$
(R9)	$HO_2 + HO_2 \rightarrow H_2O_2 + O_2$
(R10)	$NO + O_3 \rightarrow NO_2 + O_2$
(R11)	$NO_2 + h\nu \rightarrow NO + O$
(R12)	$NO_2 + OH + M \rightarrow HNO_3 + M$

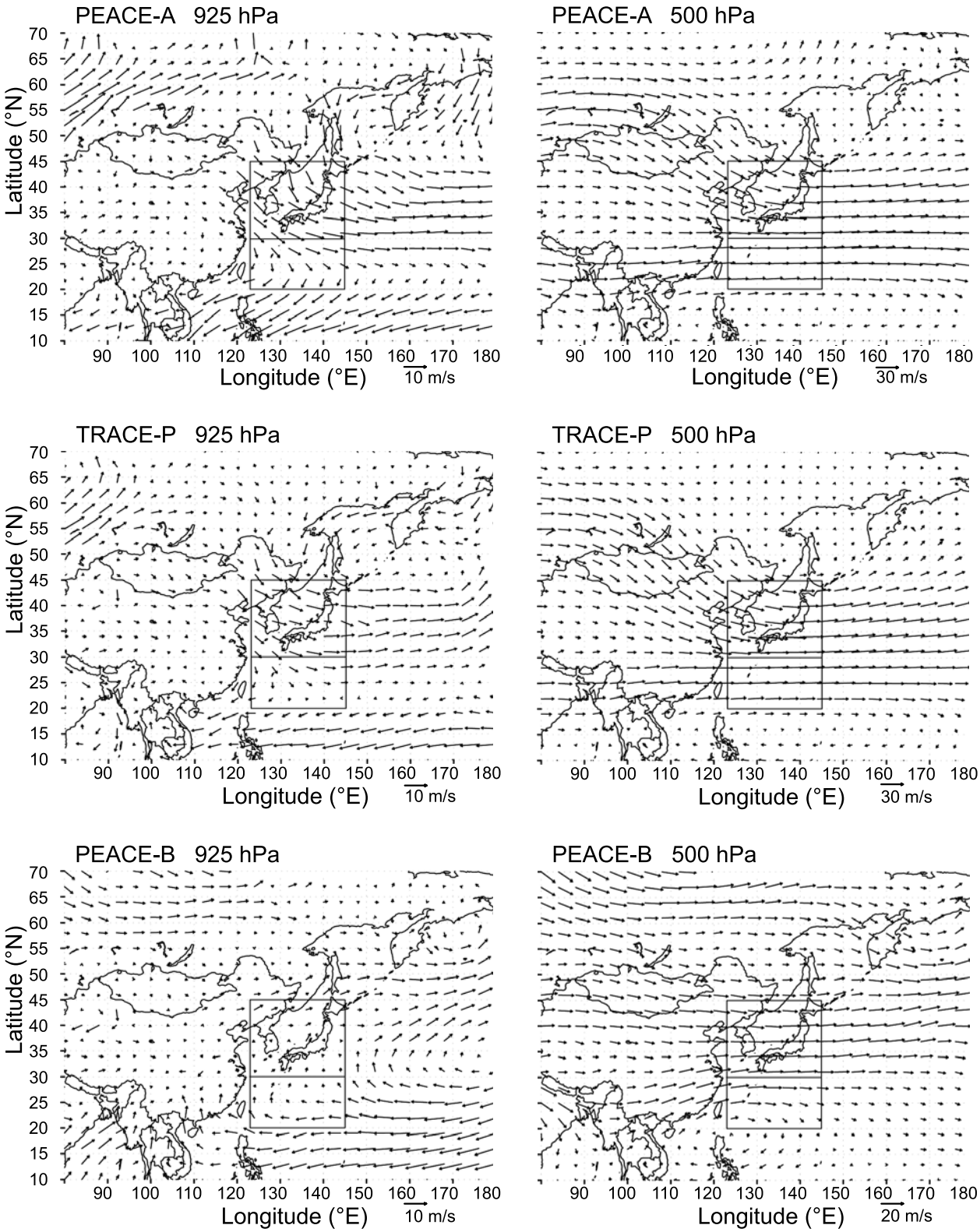

Figure 2. Mean winds at 925 and 500 hPa during PEACE-A, TRACE-P, and PEACE-B.

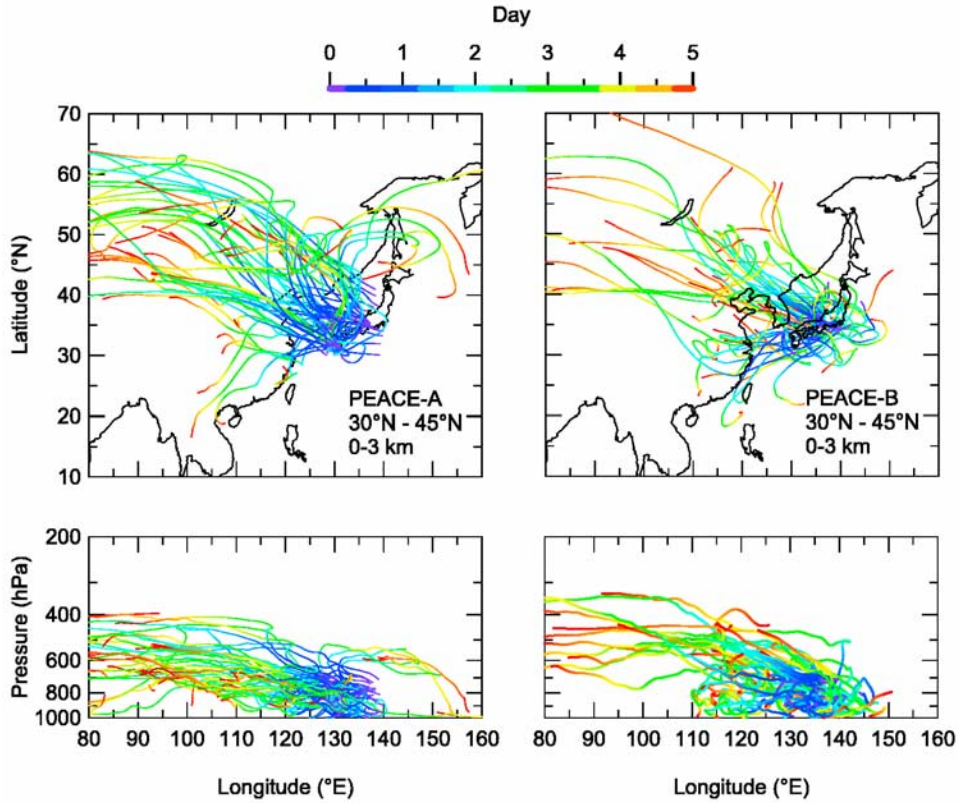

Figure 3. Five-day back trajectories of air masses sampled in the boundary layer (0–3 km) during PEACE-A and B.

with those measured during TRACE-P to within 30% [*Nakamura et al.*, 2003].

4. Meteorological Conditions in Winter and Spring

[9] Here brief descriptions of meteorological conditions relevant to the present study are given for the western Pacific region. More detailed descriptions of the meteorological conditions are given by *Fuelberg et al.* [2003] for TRACE-P and by *Oshima et al.* [2004] for PEACE-B. Mean wind fields at 925 hPa and 500 hPa during PEACE-A, TRACE-P, and PEACE-B are shown in Figure 2. The major sampling region over the western Pacific shown in Figure 1 is also shown in Figure 2. Hereafter the months of January, March, and April–May represent the observational periods for PEACE-A, TRACE-P, and PEACE-B, respectively. Seasonal variations in meteorological conditions proceeded in a different way at different latitudes (20°–30°N and 30°–45°N), as detailed below. At 925 hPa, the mean wind direction was northwesterly, and the wind speed was highest in January, because of the dominating Siberian high-pressure system. The continental outflow reached 20°N and even farther south down to 10°N during this period. The northwesterly wind weakened noticeably by March, especially at 20°–30°N. The wind speed became very weak by April–May, associated with the weakening of the Siberian high and strengthening of Pacific high pressure. The flow was easterly or southerly in the 20°–30°N region, transporting maritime air into this region. Around (30°N, 130°E), the mean wind speeds at 925 hPa in January, March, and April–May were about 8, 6, and 2 m s^{-1}, respectively (Figure 2). The boundary layer wind fields at 30°–45°N were clearly more impacted by continental outflow than those at 20°–30°N between March and May.

[10] Figure 3 shows 5-day back trajectories for air masses sampled at 30°–45°N below 3 km in January and April–May, calculated using the 1° × 1° gridded meteorological data from the European Centre for Medium-Range Weather Forecasts (ECMWF). In January, most of the sampled air masses were transported from the coastal region of the Asian continent in less than one day. In April–May, on the other hand, it took 3–5 days for most of the air masses to reach the aircraft sampling region after leaving the coastal region.

[11] At 500 hPa, northwesterly winds dominated at 30°–45°N in January and March but turned westerly by April–May. At 20°–30°N, westerlies dominated throughout the period between January and May. This latitudinal variation corresponds to the location of the subtropical jet at around 30°N. In March, vertical mixing became more active because of synoptic-scale disturbances, including transport associated with frontal systems [*Fuelberg et al.*, 2003; *Miyazaki et al.*, 2003]. Meteorological and chemical analyses have shown that most of the uplifted transport was associated with warm conveyor belts

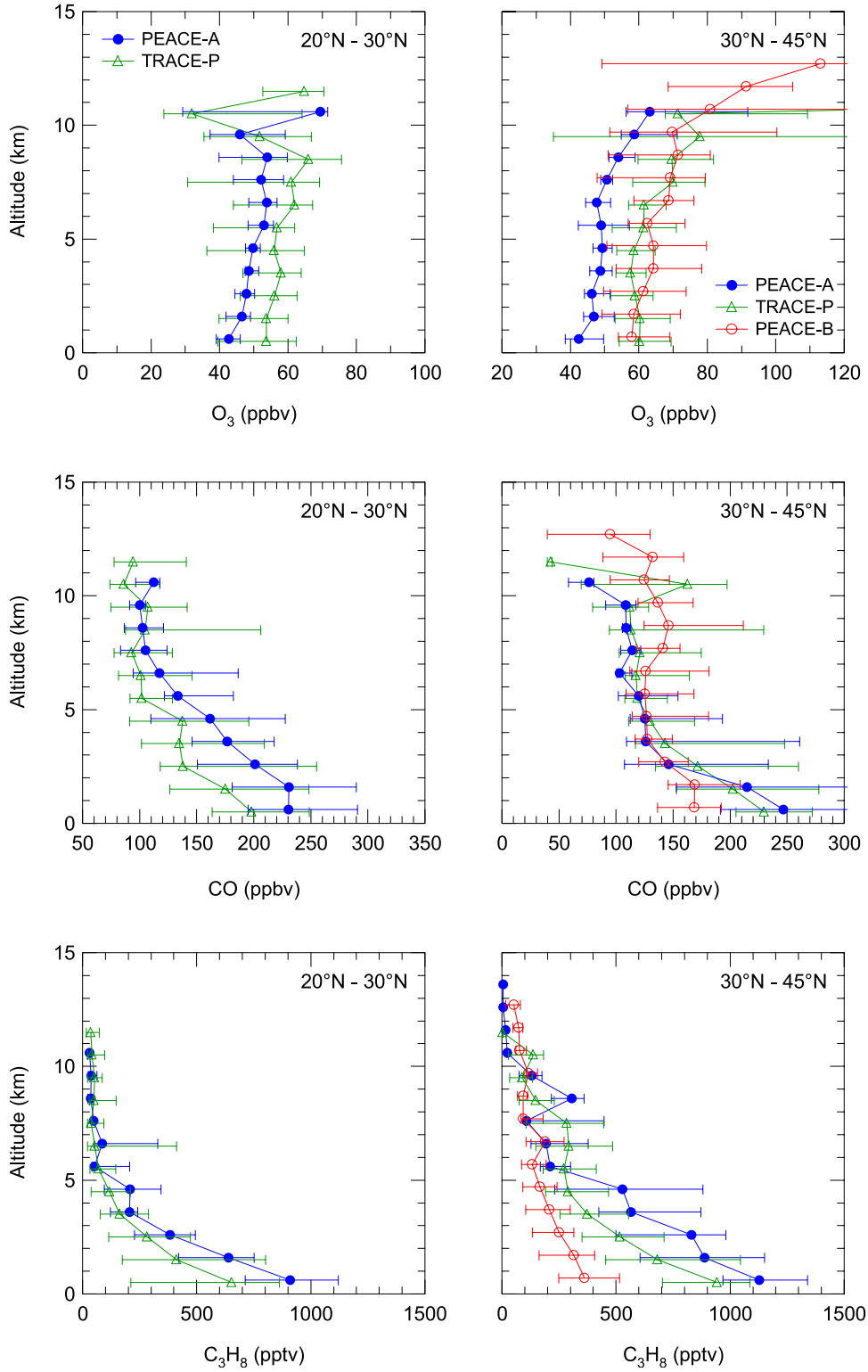

Figure 4a. Vertical profiles of the median values of O_3, CO, and C_3H_8 in the latitude ranges of (left) 20°–30°N and (right) 30°–45°N during PEACE-A, TRACE-P, and PEACE-B. Horizontal bars represent central 67 percentile values.

(WCBs) and convective outflow. In April–May, a quasi-stationary frontal zone was formed over central China by low-altitude southerlies associated with a predominant anticyclone over the central Pacific (Figure 2). Convective activities along the frontal zone occasionally transported pollutants, most prominently CO, to 6–12 km altitudes, followed by rapid eastward transport along the subtropical jet [*Oshima et al.*, 2004]. In addition to

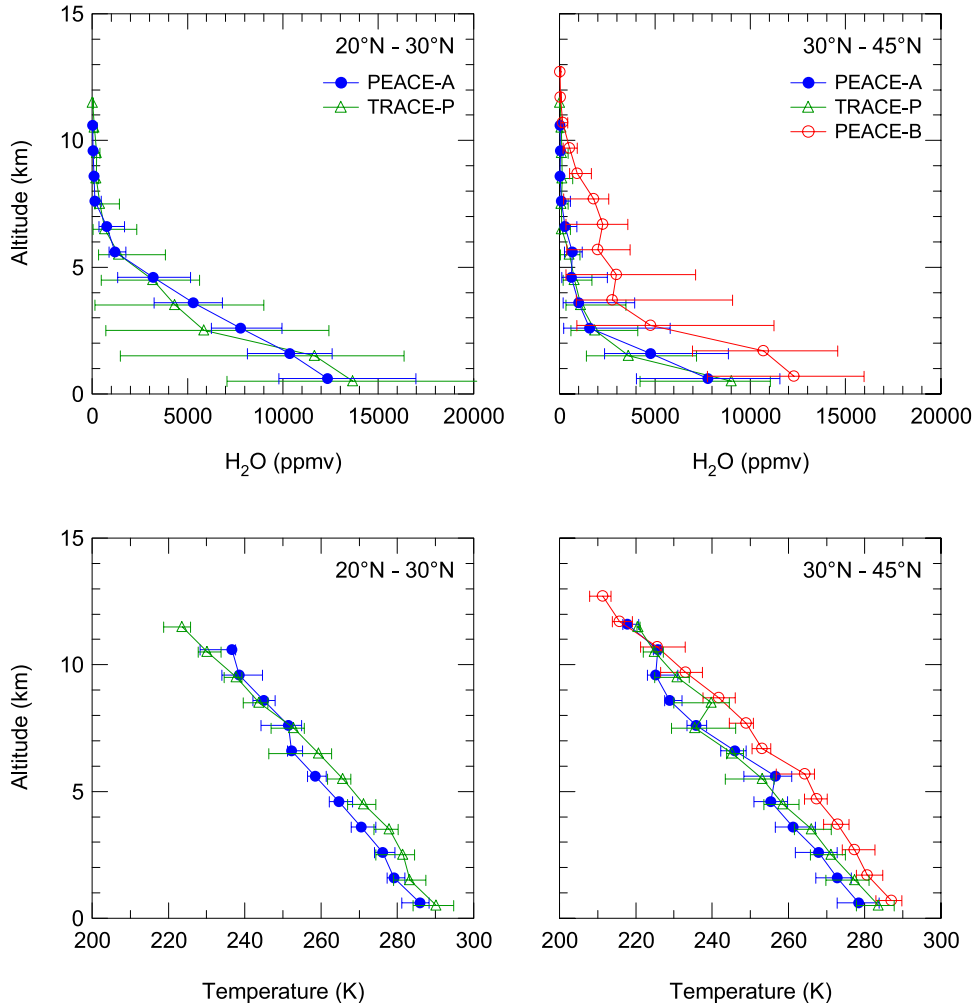

Figure 4b. Same as Figure 4a, except for vertical profiles of observed H_2O and temperature.

convection, synoptic-scale disturbances also transported pollutants to the free troposphere.

5. Seasonal and Latitudinal Variations of O_3 and Its Precursors

[12] For the present analysis, we define two latitude regions (20°–30°N and 30°–45°N) over the western Pacific at longitudes between 123°E and 145°E, considering the distinct differences in meteorological conditions between the two regions, especially in the boundary layer. In addition, both tropopause height and total O_3 column density showed abrupt changes around 30°N over the western Pacific during PEM-W-B [*Crawford et al.*, 1997] and TRACE-P [*Browell et al.*, 2003; *Wild et al.*, 2003]. The latitudinal variation of the total O_3 column strongly influences the latitudinal variation of $J(O^1D)$, which is an important controlling factor of photochemical activity. Stratospheric data were excluded by using the thermal tropopause height, which is defined as the region where the lapse rate is smaller than 2 K/2 km for a 2 km altitude range.

[13] Profiles of the median values of O_3, CO, propane (C_3H_8), H_2O, temperature, NO, NO_x (observed NO + model-calculated NO_2), and NO_x/NO_y ratio in each latitude range are shown for January, March, and April–May in Figures 4a–4c. The top of the boundary layer, as determined from the relative humidity profile, was often located between 3 and 4 km in January [*Takegawa et al.*, 2004]. This also corresponds to the altitudes where the median values of short-lived species, such as C_3H_8 and NO_x, showed sharp decreases (Figures 4a and 4c). Data with NO_x/(CO − 100 parts per billion by volume (ppbv)) exceeding 10 pptv/ppbv in the boundary layer (0–3 km) were excluded from the present analysis. These data are considered to have been strongly influenced by local NO_x emissions and do not represent regional NO_x levels. By this selection, the median NO_x mixing ratios at 0–1 km decreased by about 30%, and they changed little at 2–3 km. Column-integrated amounts of O_3 up to the tropopause are given in Table 2. It should be noted that the median values at 20°–30°N for April–May are not representative because of the very limited quantity of the data, as mentioned above, and are therefore excluded from the present analysis. The O_3 mixing ratios in the 30°–45°N regime increased at all altitudes in the troposphere from January to April–May, with major increases occurring by March. The increase was 10–20 ppbv below 8 km, depending on altitude. The increase in the total column between January and March is 2.3×10^{17} molecules cm^{-2} (28%). A similar increase

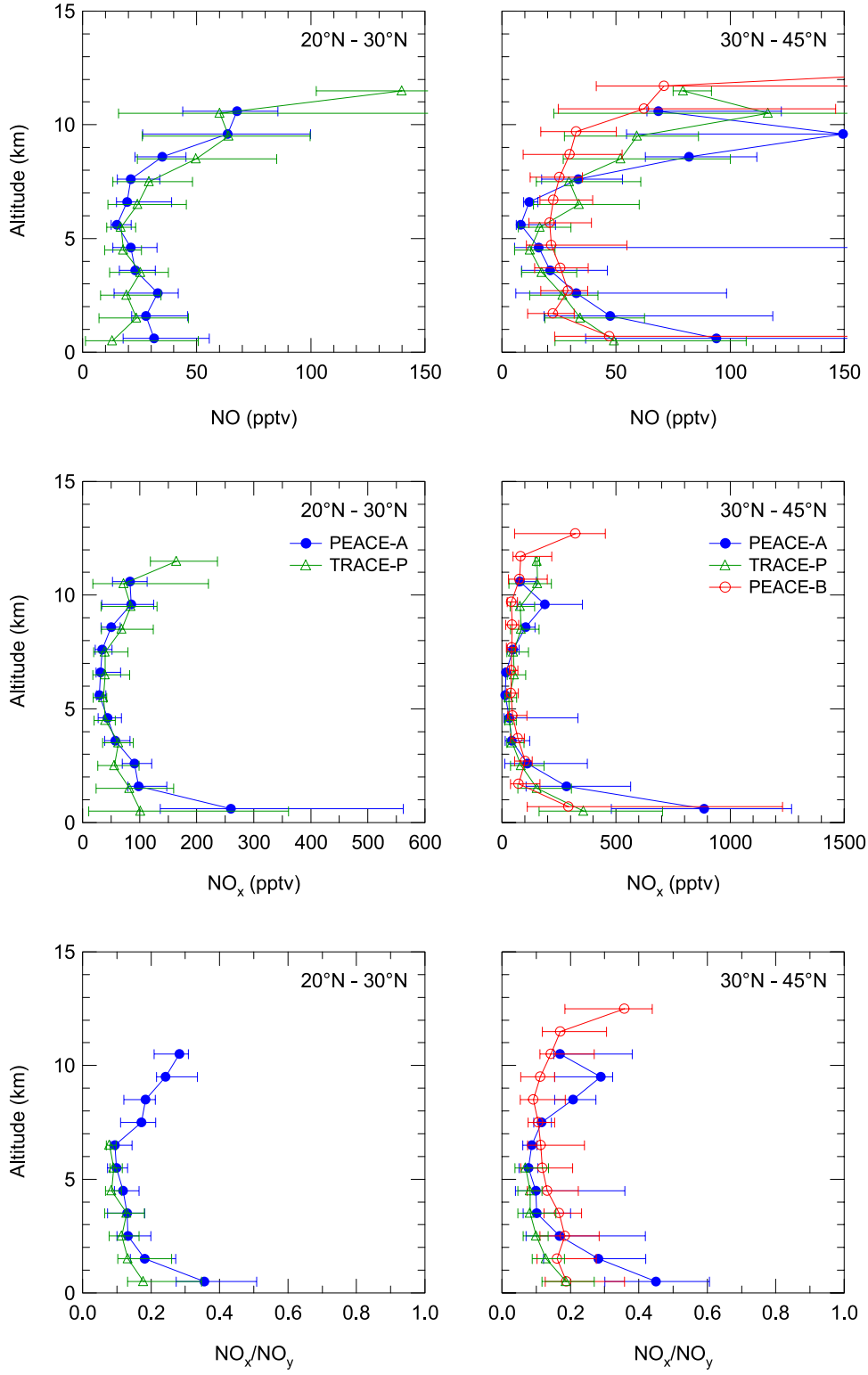

Figure 4c. Same as Figure 4a, except for vertical profiles of observed NO, NO_x, and NO_x/NO_y ratios.

was seen in the 20°–30°N regime in the same period. The median O_3 values were close to those observed by ozonesondes at three stations: Tateno (36.1°N, 140.1°E), Kagoshima (31.6°N, 130.6°E), and Naha (26.2°N, 127.7°E), operated by the Japan Meteorological Agency (JMA) (Chen et al., submitted manuscript, 2004), suggesting that the aircraft O_3 data are representative of this region. The O_3 mixing ratios in the boundary layer are plotted versus the CO mixing ratios for January and March in Figure 5. The April–May data are not shown because of the narrow range (100–200 ppbv in most cases) of CO values. The increase in O_3 from January to March is seen at similar CO values. This suggests the importance of photochemical formation of O_3 as the principal cause of the observed

Table 2. O_3 Column-Integrated Amounts[a]

20°–30°N		30°–45°N	
Altitude	O_3	Altitude	O_3
	PEACE-A		
0–3 km	3.0	0–3 km	3.0
3–6 km	2.4	3–6 km	2.4
6–12 km	2.6	6–11 km	2.8
0–12 km	8.0	0–11 km	8.2
	TRACE-P		
0–3 km	3.5	0–3 km	4.0
3–6 km	2.6	3–6 km	2.9
6–12 km	3.3	6–11 km	3.6
0–12 km	9.4	0–11 km	10.5
	PEACE-B		
0–3 km	–	0–3 km	3.9
3–6 km	–	3–6 km	3.1
6–13 km	–	6–12 km	4.2
0–13 km	–	0–12 km	11.3

[a]Units are 10^{17} molecules cm^{-2}. The highest altitude corresponds to the tropopause height, or maximum altitude of sampling if the tropopause was higher.

increase from January to March rather than transport from the stratosphere. An increase in O_3 due to stratospheric transport would be accompanied by a decrease in CO in the stratospheric air [*Singh et al.*, 1997].

[14] The CO mixing ratios below 2 km in the 30°–45°N regime were highest in January and decreased during spring. The seasonal variation of CO is mainly driven by the seasonal variation of the chemical loss rate of CO by OH and vertical mixing. Vertical mixing dilutes the high-CO boundary layer air with low-CO free tropospheric air. The vertical gradient of the CO mixing ratio was lowest in April–May, when the convection over continental regions became more frequent than in January. In fact, episodic convection associated with stationary fronts over southern China occasionally increased CO at 7–12 km in April–May, as discussed by *Oshima et al.* [2004]. The decrease in the mixing ratios from January to April–May is more systematic for C_3H_8 in the boundary layer and middle troposphere (3–6 km). In the boundary layer, C_3H_8 has a lifetime of about 13–28 (6–8) days in January (April–May), as compared to 55–110 (24–36) days for CO, as summarized in Table 3. For this calculation, the average OH concentration (also given in the table) was estimated by using a box model, as detailed in section 6.1.

[15] The H_2O mixing ratios in the 30°–45°N regime were highest in April–May because of higher temperatures. At 0.5 km, the median temperature was 278 K (287 K) in January (April–May), and the corresponding H_2O saturation mixing ratios was 0.9% (1.7%). The higher H_2O in April–May was also due to the transport of humid air from lower latitudes, associated with strengthening of the Pacific high (see Figure 2) [*Oshima et al.*, 2004]. The H_2O mixing ratios below 6 km changed little from January to March.

[16] At 30°–45°N, NO and NO_x mixing ratios at 0–2 km were highest in January. This high NO_x was caused by efficient transport of NO_x from the Asian continent due to strong winds and slow OH oxidation. The average lifetime of NO_x determined by OH oxidation is calculated to be 2.6 days (0.6 days) for January (April–May) (Table 3). *Takegawa et al.* [2004] have estimated the lifetime of NO_x in January to be 1.2 ± 0.4 days using the observed slope of the C_2H_4/C_2H_2 correlation and the OH concentration calculated by the box model. This lifetime is about 2 times shorter than the lifetime considering only oxidation by OH, suggesting the contribution of hydrolysis of N_2O_5 on aerosols ($N_2O_5 + H_2O \rightarrow 2HNO_3$). The effect of this reaction has also been studied using a 3-D model combined with the TOPSE aircraft data at midlatitudes to high latitudes over the North American continent in winter-spring [*Tie et al.*, 2003]. The relative contribution of this reaction should be greatly reduced in spring because of shorter nighttime hours and 2-to-4-times-higher OH concentrations (Table 3). In the boundary layer, the lifetime of NO_y has been estimated to be 1.7 ± 0.5 days, which is longer than but still comparable to that of NO_x (1.2 ± 0.4 days) [*Takegawa et al.*, 2004]. Because of this relatively fast removal rate of NO_y, a NO_x/NO_y ratio as high as 0.5 below 1 km is not due simply to the freshness of the air masses. The lower NO_x/NO_y ratio in spring than in January is consistent with the longer transport time. At 3–7 km, NO showed no systematic seasonal variation. The contribution of peroxyacetyl nitrate (PAN) decomposition to the observed NO_x cannot be assessed, because of the lack of PAN data during the PEACE campaigns.

[17] At 20°–30°N, the NO and NO_x mixing ratios and NO_x/NO_y ratio in the boundary layer were also higher in January than in March. The mean NO mixing ratio in January (March) was about 1–3 (1–4) times lower than that at 30°–45°N. Greater dilution and oxidation of NO_x during the longer transport time from source regions should result in the lower NO in the 20°–30°N region, downwind of the 30°–45°N region (Figure 2). The 2-times-higher OH mixing ratios at 20°–30°N (Table 3) will further enhance the NO_x oxidation and shorten its lifetime.

[18] The combined effect of the changes in transport time and OH concentrations can be seen from the C_2H_4-C_2H_2 and NO_x-CO correlations for 30°–45°N as shown in Figure 6. The lifetime of C_2H_4 in the boundary layer is 3.0 days (1.6 days) in January (March), much shorter than that of C_2H_2 (Table 3). The decrease in the C_2H_4 concentration relative to C_2H_2 indicates that air masses observed in March had undergone more processing by OH than those in winter, because of higher OH concentrations and lower wind speeds. For NO_x, correlation with CO was used instead of C_2H_2 because of the much higher sampling rate of CO and good correlation between C_2H_2 and CO. The general decrease in NO_x from January to March is seen. The change in the NO_x-CO correlation from January to March, combined with that of the C_2H_4-C_2H_2 correlation, consistently shows the important role of the oxidation of NO_x by OH in causing the observed seasonal variation in the NO_x concentrations. Hydrolysis of N_2O_5 should have reduced the degree of the change in NO_x between January and March to some extent.

6. Seasonal and Latitudinal Variations of HO_x and O_3 Photochemistry

6.1. OH and HO_2

[19] The calculated values of diurnally averaged $J(O^1D)$, $F(HO_x)$, OH, and HO_2 are shown in Figures 7a and 7b. The $J(O^1D)$ values increased from winter to spring associated with the decrease in the solar zenith angles (SZAs) as well

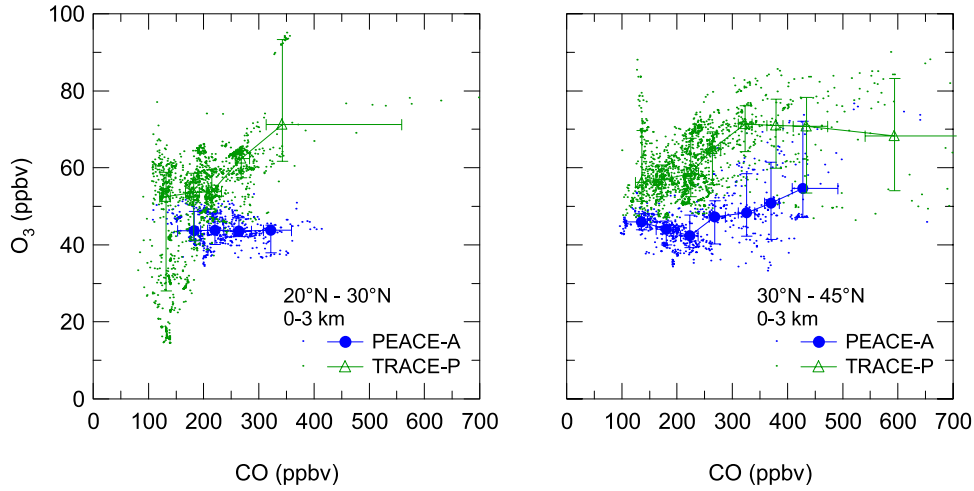

Figure 5. O_3-CO correlation observed at 30°–45°N in the boundary layer in January and March. The large circles and triangles denote median values, and the bars represent central 67 percentile values.

as the decrease in the total column O_3 density associated with the seasonal variation of stratospheric O_3. General features of the temporal and spatial variations in OH and HO_2 can be understood in terms of the variations in the $J(O^1D)$, O_3, and H_2O, which directly contribute to $F(HO_x)$ (equation (1)). Because all of these parameters increased from winter to spring in both latitude ranges, corresponding increases in OH and HO_2 are anticipated, as is shown from the calculated OH and HO_2 concentrations. The following analysis focuses mostly on the boundary layer, where the contribution to the tropospheric column-integrated O_3 formation was largest, as discussed in section 6.2.

[20] The seasonal changes in photochemistry are quite evident from the increase in HO_x levels. For example, at 30°–45°N, the OH and HO_2 concentrations at 0–12 km showed a general increase from January to March. In the boundary layer, the March/January ratio was about 2. The OH and HO_2 concentrations showed increases also from March to April–May by another factor of 2–3. The April–May/January ratios of OH and HO_2 were about 3–4 (Figure 7b). This HO_x increase is seen to be related to the seasonal increases in $F(HO_x)$, which are driven by $J(O^1D)$, O_3 and H_2O (see earlier discussion). More detailed analysis has shown the model-predicted diel average HO_x is highly correlated with $F(HO_x)$ (i.e., $r^2 > 0.7$) in all boundary layer cases, except for 30°–45°N. The lack of correlation for the latter case is due to the wide range of NO_x and NMHC levels. At the highest NO_x levels, NMHC oxidation becomes the major source of HO_x, which can be seen from the tight correlation between CH_2O and HO_x (not shown). The ratio of $[HO_2]/([HO_2] + [CH_3O_2] + [RO_2])$ was 0.6–0.7 in the boundary layer and increased to 0.8–0.9 at 8–12 km in winter and spring, indicating a limited contribution of NMHCs to peroxy radicals. Similar results have been obtained by *Davis et al.* [2003] for the TRACE-P March data.

[21] At 20°–30°N, the OH and HO_2 concentrations also increased from January to March. This increase is mainly due to the increase in $F(HO_x)$ as a result of shifts in $J(O^1D)$ and O_3, while the H_2O mixing ratios showed little changes. In March, the OH and HO_2 concentrations in the boundary layer at 20°–30°N were higher than those at 30°–45°N by factors of 1.5–3. The difference in $J(O^1D)$ and H_2O is the major reason, because the O_3 concentrations were similar.

6.2. Net Ozone Formation

[22] Calculated values of $F(O_3)$, $D(O_3)$, and $P(O_3)$ integrated for each 1 km altitude range are shown in Figure 8 for three observation periods for each latitudinal range. The column-integrated values are given in Table 4. The $P(O_3)$ profile at 30°–45°N in units of ppbv d^{-1} is shown in Figure 9. The relative contribution of each reaction term to $F(O_3)$ and $D(O_3)$ is given in Tables 5 and 6. It should be noted that $F(O_3)$ and $D(O_3)$ are directly connected through HO_2 and indirectly through $J(O^1D)$ and H_2O, which control HO_x (equations (2) and (3)).

6.2.1. The 30°–45°N Regime

6.2.1.1. Boundary Layer

[23] At 30°–45°N, $F(O_3)$ and $D(O_3)$ values in the boundary layer were largest in April–May, reflecting the highest photochemical activities, as represented in the HO_x concentrations. However, the $F(O_3)$ values for January were smaller than those for April–May by only 35%, despite the difference of a factor 3 in HO_2, which directly influences $F(O_3)$ (equation (2)). This difference is compensated by the 2-times-larger NO mixing ratios in January. The contribution of reaction (R4) to $F(O_3)$ is proportional to the

Table 3. Lifetimes of CO, NMHCs, and NO_x in the Boundary Layer Determined by the Reactions With OH for PEACE-A, TRACE-P, and PEACE-B[a]

	20°–30°N			30°–45°N		
Species	PEACE-A	TRACE-P	PEACE-B	PEACE-A	TRACE-P	PEACE-B
CO	42.0	31.2	–	119.6	60.2	24.6
C_2H_6	49.6	34.6	–	154.4	74.2	28.3
C_2H_4	1.2	0.9	–	3.3	1.7	0.7
C_2H_2	14.4	10.4	–	42.9	21.1	8.3
C_3H_8	10.0	7.1	–	30.0	14.7	5.8
n-C_4H_{10}	4.1	2.9	–	12.2	6.0	2.4
NO_x	1.0	0.8	–	2.6	1.4	0.6
OH	12.1	16.5	–	4.3	8.5	20.9

[a]Units are days. OH is given in units of 10^5 molecules cm^{-3}.

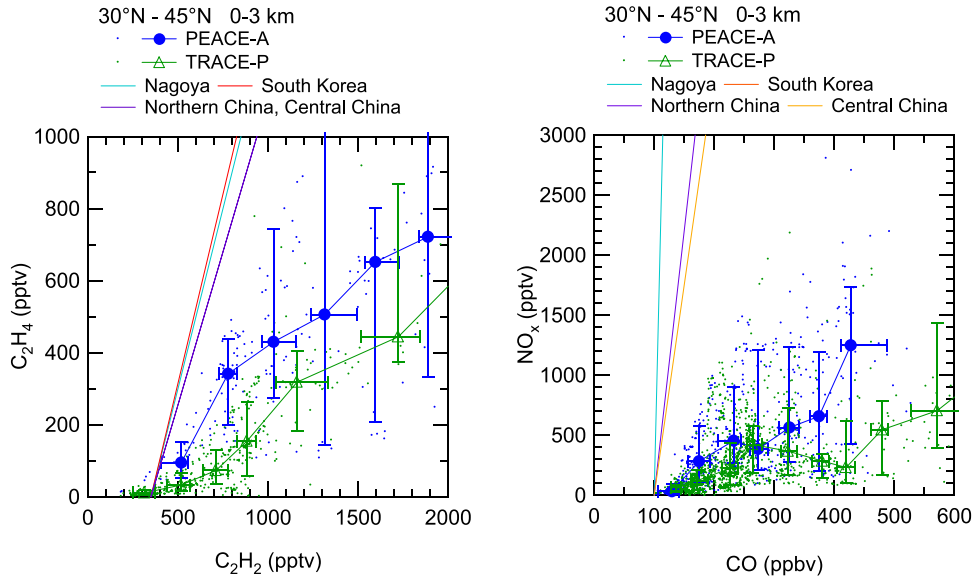

Figure 6. Same as Figure 5, except for C_2H_4-C_2H_2 and NO_x-CO correlations. Correlations derived from the emissions of C_2H_2, CO, C_2H_4, and NO_x, estimated by *Streets et al.* [2003] for Nagoya (Japan), South Korea, northern China, and central China are also shown for comparison (thin lines).

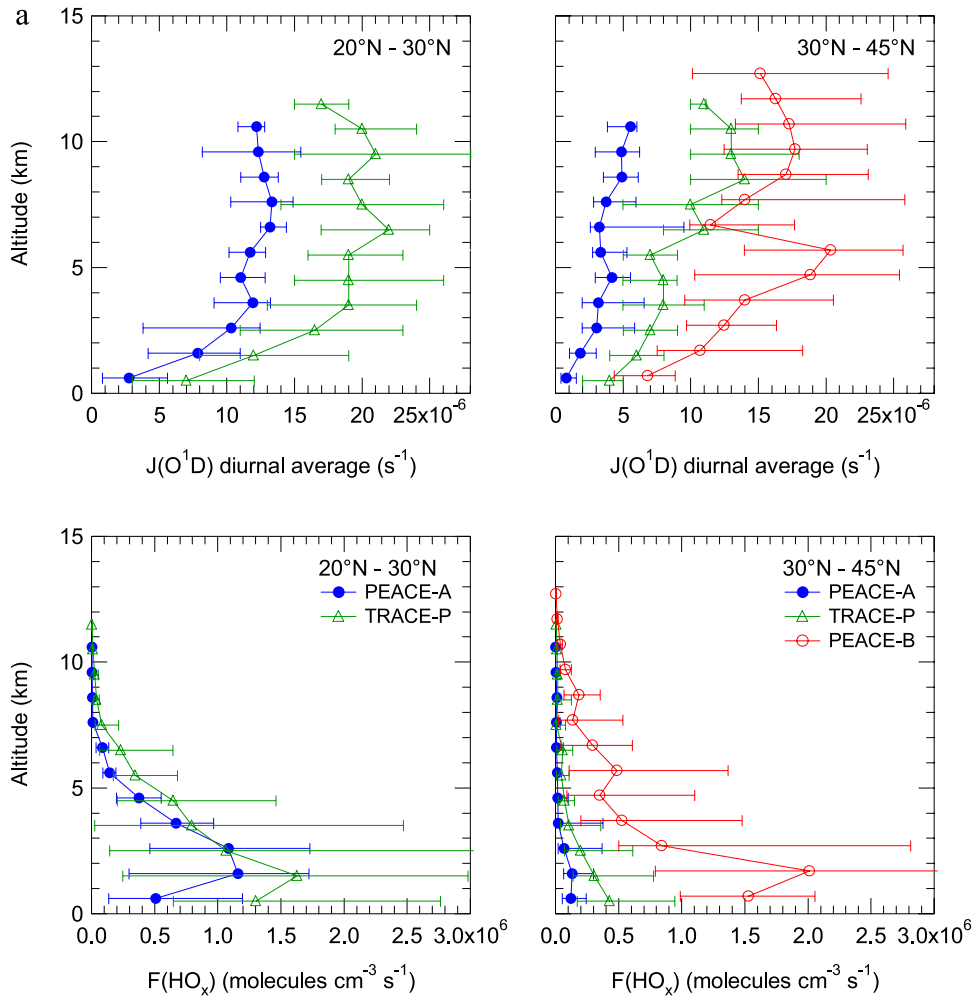

Figure 7. (a) Same as Figure 4a, except for vertical profiles of the 24-hour average $J(O^1D)$ and $F(HO_x)$; (b) OH and HO_2.

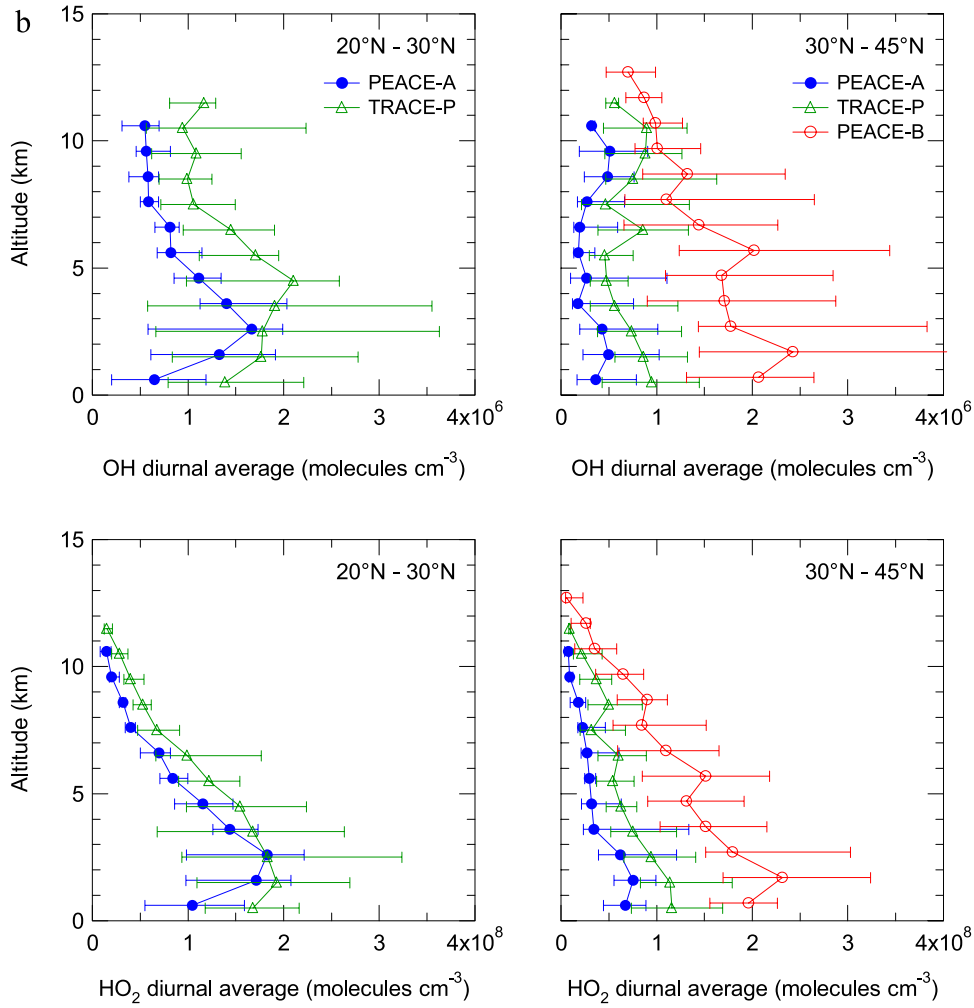

Figure 7. (continued)

$[HO_2]/([HO_2] + [CH_3O_2] + [RO_2])$ ratio, which was 60–70% in the boundary layer, as summarized in Table 5.

[24] Although the $F(O_3)$ values showed only modest increases from winter to spring, the $D(O_3)$ values increased much more rapidly. This increase occurred most dramatically between March and April–May. The $D(O_3)$ values for January were 2 times lower than those for March and 5 times lower than those for April–May. In January, reaction (R8) made a major contribution to the total $D(O_3)$, and the contribution of reaction (R3a) was only 30%. The contribution of reaction (R3a) to $D(O_3)$ increased to about 50% in April–May (Table 6). The largest values of $D(O_3)$ in April–May were due to the largest values of the parameters controlling $D(O_3)$ given in equation (3), namely, O_3, $J(O^1D)$, H_2O, HO_2, and OH.

[25] Because $F(O_3)$ is proportional to [NO], $F(O_3)$ and $D(O_3)$ balance at a specific level of NO, defined as the critical NO (NO_{crit}) [*Crawford et al.*, 1997; *Davis et al.*, 2003]. When the ambient NO levels are higher than NO_{crit}, photochemistry tends to be a net source of O_3. Conversely, the photochemistry is a net sink when NO is low. The value of NO_{crit} depends on the value $D(O_3)$, which increases with photochemical activity and O_3. The calculated NO_{crit} is shown in Figure 10. NO_{crit} increased from January (9 pptv) to April–May (29 pptv), corresponding to the seasonal variation of the photochemical activity.

[26] The $P(O_3)$ value in the boundary layer was largest in January, because of $F(O_3)$ comparable to that in spring and much lower $D(O_3)$. The $P(O_3)$ value decreased by 25% from January to March, and by April–May, it decreased down to about 10% of the January value (Table 4). The net O_3 production in the boundary layer was a major contributor to the total column production: about 80% for January and 30% for March–May (Table 4). The fact that $P(O_3)$ was positive during January–March and was much reduced in the April–May period is consistent with the largest increase in O_3 during the January–March period and the smaller change during the March–May period (Table 2).

6.2.1.2. Middle Troposphere

[27] The $P(O_3)$ values were lowest in the middle troposphere (3–6 km) during all the three periods (Figures 8 and 9). Specifically in April–May, both $F(O_3)$ and $D(O_3)$ monotonically decreased with altitude, and the middle tropospheric values were smaller than those in the boundary layer by only a factor of 2–3 (Table 4). The $F(O_3)$ and $D(O_3)$ in the middle troposphere contributed 24% of the column-integrated values. However, contribution of $P(O_3)$ in this region to the total integrated value amounted to only

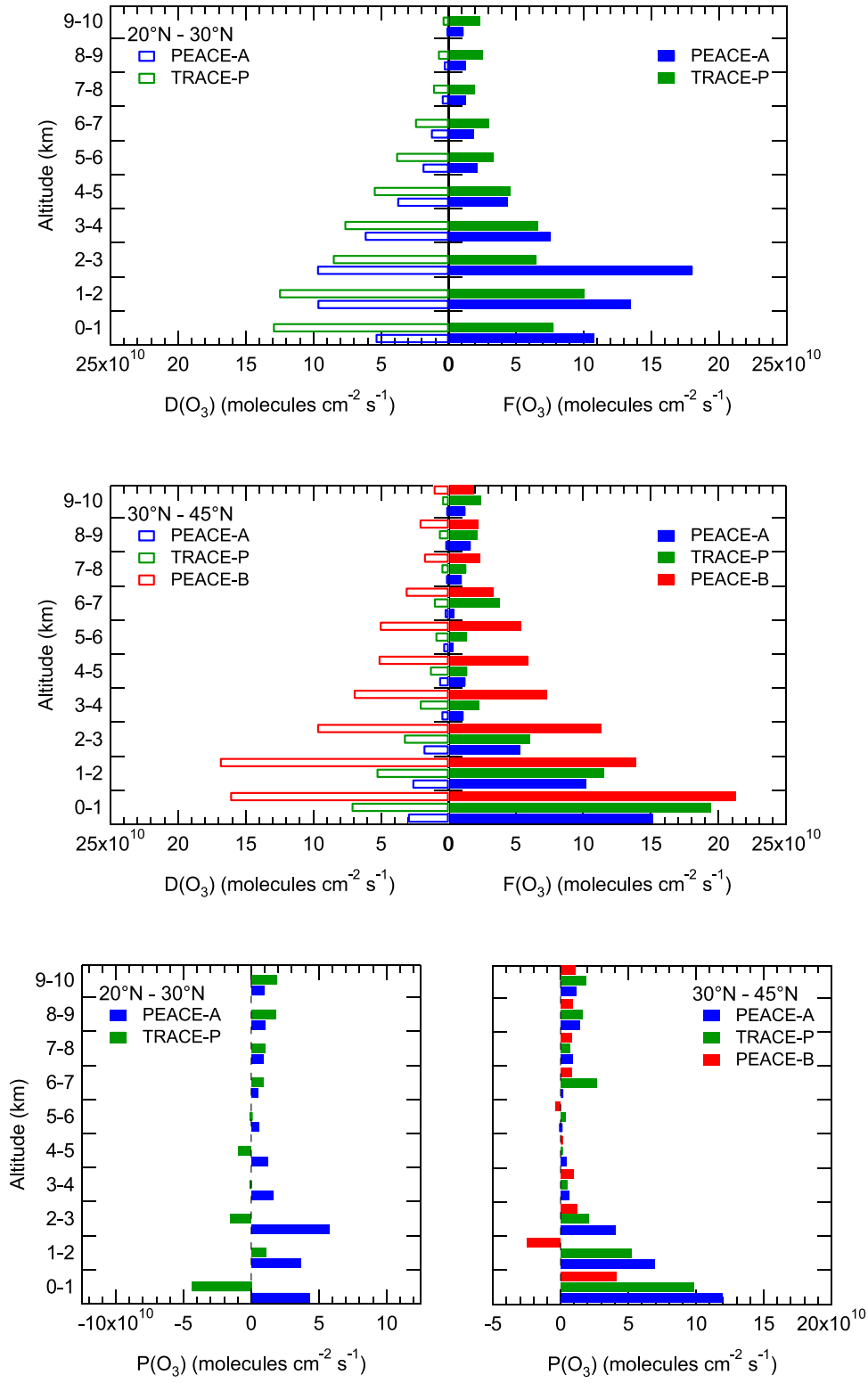

Figure 8. Vertical profiles of the O_3 formation ($F(O_3)$), destruction ($D(O_3)$), and net formation ($P(O_3)$) rates in the latitude ranges of 20°–30°N and 30°–45°N during PEACE-A, TRACE-P, and PEACE-B.

Table 4. Column-Integrated Values of $F(O_3)$, $D(O_3)$, and $P(O_3)$[a]

20°–30°N				30°–45°N			
Altitude	$F(O_3)$	$D(O_3)$	$P(O_3)$	Altitude	$F(O_3)$	$D(O_3)$	$P(O_3)$
			PEACE-A				
0–3 km	42	25	14	0–3 km	31	7.6	23
3–6 km	14	12	3.4	3–6 km	2.9	1.7	1.1
6–11 km	6.7	2.6	4.2	6–11 km	5.0	1.1	4.0
0–11 km	63	39	21	0–11 km	39	10	28
			TRACE-P				
0–3 km	24	34	−4.8	0–3 km	37	16	17
3–6 km	15	17	−1.1	3–6 km	5.2	4.5	0.98
6–12 km	14	5.5	8.7	6–11 km	12	3.3	8.0
0–12 km	53	57	2.8	0–11 km	54	24	26
			PEACE-B				
0–3 km	37	48	–	0–3 km	47	43	2.9
3–6 km	35	51	–	3–6 km	19	17	0.80
6–13 km	35	17	–	6–12 km	13	9.3	5.7
0–13 km	107	116	–	0–12 km	78	70	9.4

[a]Units are 10^{10} molecules cm^{-2} s^{-1}.

Table 5. Percentage Contribution of Different Peroxy-Radicals to O_3 Formation at 30°–45°N for January, March, and April–May[a]

	HO_2			CH_3O_2			RO_2		
Altitude, km	J	M	A–M	J	M	A–M	J	M	A–M
0–3	62	70	66	12	15	20	24	15	12
3–6	70	73	72	16	17	20	13	9	8
>6	83	82	81	11	12	11	6	6	8

[a]J, M, and A–M stand for January, March, and April–May, respectively.

9%. The $P(O_3)$ values were observed to be lowest in the middle troposphere also in September during PEM-W-A [*Davis et al.*, 1996; *Crawford et al.*, 1997].

[28] The lifetime of O_3 in the middle troposphere at 30°N in January and July is estimated to be 100 and 20 days, respectively, by a 3-D chemical transport model (CTM) [*Wang et al.*, 1998b]. This is much longer than the corresponding lifetimes of 40 and 6 days in the boundary layer. Therefore O_3 in the boundary layer should tend to be closer to photochemical steady state in general. The large departure from photochemical steady state in the boundary later is due to active input of NO_x from the Asian continent. Values closer to photochemical steady state in the middle troposphere should be due to the minimal NO_x levels, owing to the lack of in situ sources and longer transport time of NO_x from source regions below and above.

6.2.1.3. Upper Troposphere

[29] In the upper troposphere (6–12(±1) km), O_3 deviated from photochemical steady state as in the boundary layer. The $F(O_3)$ values increased or remained unchanged with altitude from the middle to the upper troposphere, while the $D(O_3)$ values decreased. The causes in the altitude changes in $F(O_3)$ and $D(O_3)$ are the increase in NO and the decrease in H_2O concentrations with altitude, respectively. Even in April–May, when H_2O was highest, the contribution of reaction (R3a) to $D(O_3)$ was not dominant. As a result of these changes, $P(O_3)$ was positive in the upper troposphere because of "excess NO" above NO_{crit} (Figure 10). The $P(O_3)$ integrated in the upper troposphere contributed about 14% and 60% of the column-integrated $P(O_3)$ values in January and April/May, respectively. Over the western Pacific, net O_3 formation in the upper troposphere was also observed in September and February during PEM-W-A and B [*Davis et al.*, 1996; *Crawford et al.*, 1997]. The median NO mixing ratios at 10–12 km during these periods were 40–100 pptv, which are similar to those observed in January, March, and April–May. The persistent net O_3 formation throughout the year has been predicted by 3-D CTMs [*Wang et al.*, 1998b; *Yienger et al.*, 1999].

[30] The major sources of NO in the upper troposphere are known to be production by lightning, emissions from commercial aircraft, transport of NO_x from the boundary layer, and transport of HNO_3 from the stratosphere followed by reaction with OH and photolysis to form NO_x [*World Meteorological Organization*, 1999]. The NO emissions from aircraft are concentrated at northern midlatitudes, while lightning activity is highest in the tropics [e.g., *Levy et al.*, 1999; *Lamarque et al.*, 1996]. The effect of air traffic on upper tropospheric NO_x was indicated over the western Pacific during PEM-W-B, where air traffic is frequent [*Koike et al.*, 1997]. High NO_x observed in the upper troposphere was often correlated with high condensation

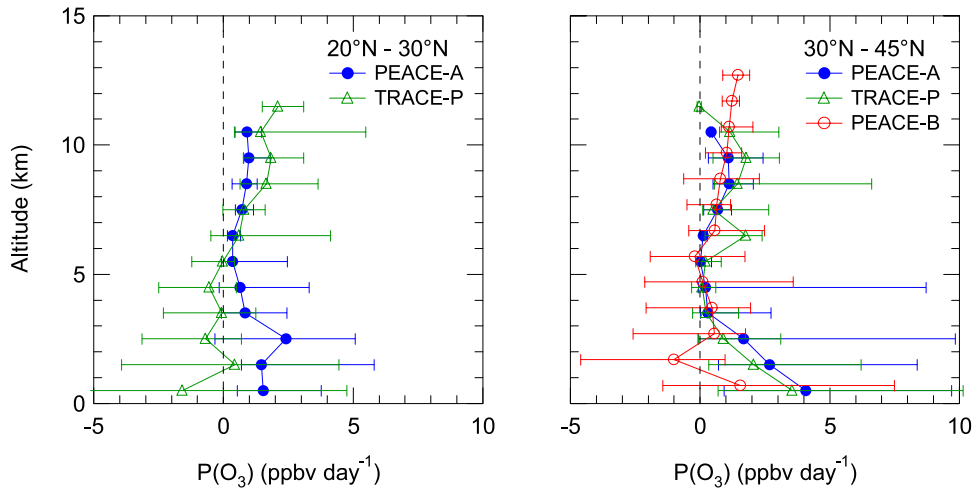

Figure 9. Vertical profiles of the net formation ($P(O_3)$) rate at 20°–30°N and 30°–45°N in units of ppbv d^{-1}.

Table 6. Percentage Contribution of Different Reactions to O_3 Destruction at 30°–45°N for January, March, and April–May[a]

Altitude, km	$O(^1D)$			$HO_2 + O_3$			OH + O_3			NO_2 + OH		
	J	M	A–M	J	M	A–M	J	M	A–M	J	M	A–M
0–3	27	30	49	47	48	33	11	13	13	13	5	3
3–6	15	26	39	64	56	42	14	15	16	2	1	1
>6	12	15	33	46	42	39	36	32	27	5	3	1

[a]J, M, and A–M stand for January, March, and April–May, respectively.

nuclei (CN) densities. Similar correlation was observed in the North Atlantic flight corridor during the SASS Ozone and NO_x Experiment (SONEX) [*Kondo et al.*, 1999]. This excludes a large contribution of transport of stratospheric HNO_3 to the observed high NO_x, because HNO_3 from the stratosphere does not correlate with CN in general. This in itself does not exclude convective transport of NO_x and CN from the boundary later, however. NO_x-CO and NO_y-CO correlations were generally poor, but occasionally significant (not shown), suggesting some effect of transport from the boundary layer. The number of data points obtained in the upper troposphere was considerably smaller than that in the boundary layer and middle troposphere. This prevents the use of statistical analysis to quantify contributions of different sources of NO_x in the upper troposphere.

6.2.2. The 20°–30°N Regime

6.2.2.1. Boundary Layer

[31] Changes in the $F(O_3)$, $D(O_3)$, and $P(O_3)$ values in the 20°–30°N regime are discussed in comparison with those in the 30°–45°N regime. In January, the $F(O_3)$ values in the boundary layer at 20°–30°N were 25% higher than those at 30°–45°N (Figure 5 and Table 3). The median NO mixing ratios at 20°–30°N were about 1–3 times lower than those at 30°–45°N, as discussed in section 5. The effect of lower NO concentrations at 20°–30°N is compensated by the 2-to-3-times-higher HO_2 (Figures 4c and 7a–7b), because of much higher $F(HO_x)$ values in this latitude bin. The $D(O_3)$ values at 20°–30°N were 3 times higher than those at 30°–45°N, mostly because of the larger values of $J(O^1D)$ and H_2O. The resulting $P(O_3)$ values at 20°–30°N turned out to be positive. In March, the $P(O_3)$ values became negative. The decrease in $F(O_3)$, mainly due to the decrease in NO, and the increase in $D(O_3)$ are together the major cause of the large decrease in $P(O_3)$ from January. The decrease in NO, in turn, was caused by a higher fraction of Asian NO_x oxidized because of the much weaker winds, especially at 20°–30°N (Figure 2), and

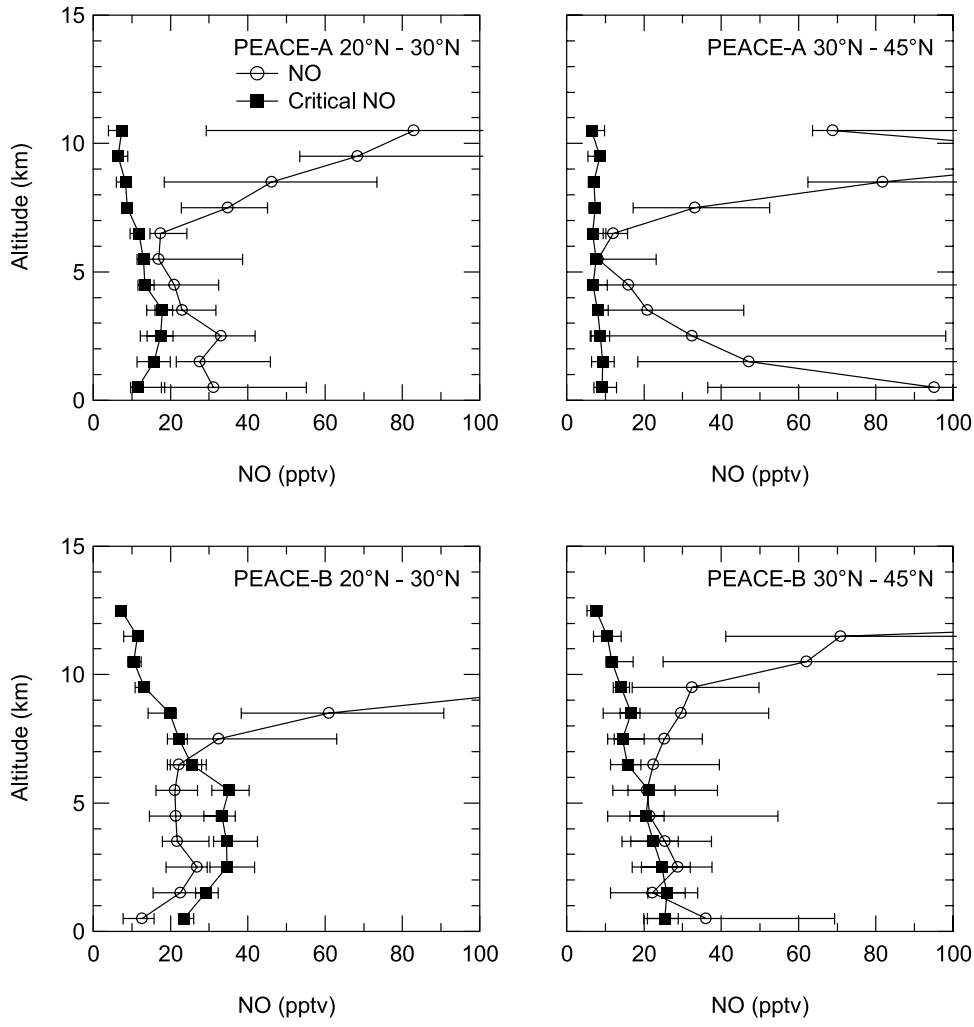

Figure 10. Vertical profiles of the median values of the observed and critical NO mixing ratios.

Table 7. Integrated Values of $F(O_3)$, $D(O_3)$, and $P(O_3)$ and Median Values of NO_x, H_2O, and $J(O^1D)$ in the Boundary Layer at 40°–60°N During TOPSE[a]

	February (PEACE-A)	March (TRACE-P)	April (PEACE-B)	May
$F(O_3)$	3.7 (31)	8.8 (37)	12 (47)	14
$D(O_3)$	2.6 (7.6)	8.2 (16)	11 (43)	17
$P(O_3)$	0.9 (23)	1.8 (17)	2.1 (2.9)	−2.4
NO_x, pptv	27 (419)	34 (190)	42 (130)	44
H_2O, ppmv	1410 (4080)	2770 (4840)	2240 (9960)	3710
$J(O^1D)$	1.1 (1.9)	3.4 (5.7)	5.0 (10)	8.7

[a]Units for $F(O_3)$, $D(O_3)$, and $P(O_3)$ are 10^{10} molecules cm^{-2} s^{-1}, and those for $J(O^1D)$ are 10^{-6} s^{-1}. The numbers in parentheses are the values for 30°–45°N over the western Pacific.

higher OH levels (Figures 7a–7b) than in January, as discussed in section 5. The $P(O_3)$ value integrated over the boundary layer is -4.8×10^{10} molecules cm^{-2} s^{-1}.

[32] In February–March during PEM-W-B, $P(O_3)$ was positive in the boundary layer [*Crawford et al.*, 1997]. PEM-W-B was conducted about three weeks earlier than TRACE-P. The values of $F(O_3)$, $D(O_3)$, and $P(O_3)$ integrated over 0–4 km were 39×10^{10}, 28×10^{10}, and 11×10^{10} molecules cm^{-2} s^{-1}, respectively. These values are comparable to those integrated over 0–3 km for January (Table 4). The median NO mixing ratio during PEM-W-B was about 20 pptv, which is comparable to the values in January, leading to the comparable $F(O_3)$ values. The $F(O_3)$ and $D(O_3)$ during PEM-W-B were higher and lower than those in March, respectively, resulting in the difference in the sign of $P(O_3)$. The lower $D(O_3)$ during PEM-W-B was due mainly to the lower $J(O^1D)$, as H_2O and HO_x concentrations were similar. By comparing the results for January, February–March, and March, it appears that $P(O_3)$ turned from positive to negative sometime between February and March, one month earlier than at 30°–45°N. The earlier change in the sign of $P(O_3)$ is due to the earlier decrease in NO (leading to decrease in $F(O_3)$) and earlier increases in $J(O^1D)$ and H_2O (leading to increase in $D(O_3)$).

6.2.2.2. Middle and Upper Troposphere

[33] In January, $F(O_3)$ values in the middle troposphere were larger than those at 30°–45°N, because of the higher HO_2 and comparable NO levels. The $D(O_3)$ values at 20°–30°N were 3–4 times higher than those at 30°–45°N, because of the larger values of $J(O^1D)$, H_2O, HO_2, and OH. The resulting $P(O_3)$ values at 20°–30°N turned out to be 2 times larger. In March, the $P(O_3)$ values in the middle troposphere became negative, similarly to the boundary layer.

[34] In January and March, the $P(O_3)$ values in the upper troposphere at 20°–30°N were similar to those at 30°–45°N. The NO levels in both latitude regimes were similar (Figure 4c).

6.2.3. Influx From the Stratosphere and Surface Deposition

[35] Studies have shown that transport from the stratosphere and dry deposition on the Earth's surface can also have significant contributions to tropospheric O_3, in addition to photochemical formation and destruction. Chemical destruction and deposition affect O_3, regardless of its origin, namely tropospheric or stratospheric. Thus it is appropriate to compare the O_3 transport term with $F(O_3)$. The effect of O_3 from the stratosphere on the O_3 budget has been assessed in some detail by *Davis et al.* [2003] by comparing O_3 fluxes estimated by previous studies with derived column-integrated $F(O_3)$ values at 25°–45°N for the PEM-W-B (February–March) and TRACE-P (March) data. Column-integrated $F(O_3)$ values of 28×10^{10} and 54×10^{10} molecules cm^{-2} s^{-1} for February–March and March, respectively, were 3–6 times larger than the O_3 flux from the stratosphere of 8.7×10^{10} molecules cm^{-2} s^{-1}, estimated for the latitude range of 20°–60°N by *Wang et al.* [1998a]. Photochemistry dominates over influx from the stratosphere. The same conclusion applies to the present data sets because $F(O_3)$ values in January and April–May in the range at 20°–30°N and 30°–45°N were between 39×10^{10} and 78×10^{10} molecules cm^{-2} s^{-1}, which is 4–9 times higher than the flux from the stratosphere.

[36] The integrated $D(O_3)$ at 30°–45°N were 10×10^{10}, 24×10^{10}, and 70×10^{10} molecules cm^{-2} s^{-1} for January, March, and April–May, respectively. The average surface deposition of 5×10^{10} molecules cm^{-2} s^{-1} estimated by *Kawa and Pearson* [1989] and *Lenschow et al.* [1982] becomes comparable to the chemical destruction for January, the period of the minimum photochemical activity. However, the integrated $P(O_3)$ value of 28×10^{10} molecules cm^{-2} s^{-1} for January is not significantly altered by taking the deposition into account because of the much higher value of $F(O_3)$ than $D(O_3)$ and surface deposition (Table 4).

6.3. Implications of the Present Data and Comparison With TOPSE

[37] The present data were obtained in the region about 200–2000 km distant from the coast of the Asian continent. This is the region over the Pacific most significantly influenced by anthropogenic activities in Asia, as indicated by previous studies using 3-D CTMs [e.g., *Wang et al.*, 1998a; *Yienger et al.*, 1999]. At farther distance from the continent, concentrations of short-lived precursors, especially NO_x, are predicted to decrease greatly because of oxidation and dilution, as was observed during PEM-W-A and B [*Kondo et al.*, 1997]. Accordingly, O_3 photochemistry, especially the $F(O_3)$ value, should be much reduced in more remote regions of the Pacific. The seasonal variation of $P(O_3)$ shown here, therefore, should be interpreted to represent that in the region close enough to sources, where precursor concentrations, especially NO_x, are still high. The total O_3 formed within 3.5 months from January to April–May is calculated to be 19×10^{17} molecules cm^{-2}, assuming an average column-integrated $P(O_3)$ of 21×10^{10} molecules cm^{-2} s^{-1} during this period. This O_3 formation is 6 times larger than the observed increase in the O_3 column of 3.1×10^{17} molecules cm^{-2} during this period, indicating that O_3 formed over the western Pacific was transported to regions over the Pacific outside the region of the present study. Namely, O_3 formed in this study area can cause similar seasonal increase in O_3 in a region 5 times larger than this area.

[38] Similar seasonal variation of $P(O_3)$ can prevail downwind of other continental sources, as predicted by 3-D CTMs [e.g., *Yienger et al.*, 1999], because the parameters $J(O^1D)$, H_2O, OH, HO_2, and wind fields, which control $P(O_3)$, are considered to follow similar seasonal variations.

They are mainly driven by natural seasonal variations. In this regard, there can be other regions where the seasonal variation of the O_3 chemistry is driven by natural changes in these parameters coupled with anthropogenic emissions of O_3 precursors, in a way similar to that over the western Pacific.

[39] Seasonal variations of the O_3 photochemistry from February to May over the North American continent were also calculated with a time-dependent photochemical box model using TOPSE aircraft measurement data as input parameters [*Wang et al.*, 2003; *Stroud et al.*, 2004], in a similar way to that of the present study. Monthly median values of $F(O_3)$, $D(O_3)$, $P(O_3)$ in the boundary layer, and key parameters (NO_x, H_2O, and $J(O^1D)$) controlling O_3 photochemistry are listed in Table 7 for the latitude band of 40°–60°N. TOPSE NO_x observations at 0–3 km at midlatitudes (40°–60°N) (Table 7) did not show a large seasonal variation from January to May.

[40] The H_2O mixing ratios were also 2–3 times lower over North America, due primarily to the lower temperature. In addition, airflow over North American orography leads to much drier conditions in the boundary layer. The values of H_2O and $J(O^1D)$ over North America increased from winter to spring, leading to increases in both $F(O_3)$ and $D(O_3)$ of comparable size. As a consequence, $P(O_3)$ from February to April was stable. By contrast, over the western Pacific, a large decrease in NO_x and increase in H_2O from winter to spring caused large decreases in $P(O_3)$, as discussed in section 6.2.1. The $F(O_3)$ values in the TOPSE study region were 4–8 times lower than those over the western Pacific because of the correspondingly lower NO_x values. The $P(O_3)$ values were about 20 times lower in the January–March period. Differences in the values of H_2O and $J(O^1D)$ make additional contributions to the differences in $P(O_3)$. This comparison, based on measured key parameters, demonstrates the critical role of NO_x in controlling O_3 production on regional scales.

7. Conclusions

[41] Seasonal variations of solar UV radiation ($J(O^1D)$) and concentrations of key precursors (NO, H_2O, OH, and HO_2) determine the seasonal variations of chemical O_3 formation and destruction. In the boundary layer over the western Pacific (123°–145°E), H_2O and HO_x increased primarily because of increases in temperature and solar radiation and NO_x decreased primarily because of decrease in transport efficiency from the Asian continent from winter to spring. The changes of these key parameters are coupled in the O_3 chemistry. The complex chemical interplay over the western Pacific during this period has been assessed systematically using box model calculations constrained by the data sets obtained by aircraft observations made in the latitude regimes of 20°–30°N and 30°–45°N in January (PEACE-A), March (TRACE-P), and April–May (PEACE-B).

[42] At 30°–45°N, the OH concentration of $0.2–0.5 \times 10^6$ molecules cm^{-3} in the boundary layer (0–3 km) and middle troposphere (3–6 km) almost doubled by March. It showed a factor of 2–3 increase from March to April–May, due to the increase in $J(O^1D)$ and H_2O. This leads to a shortening of lifetimes by a factor of 4 of trace species that are removed by reaction with OH, from winter to late spring.

[43] In this latitude range, NO concentration in the boundary layer was highest in January because of the strongest outflow of dry polluted air from the Asian continent under the influence of the Siberian high. This high NO was compensated by low HO_2 due to low H_2O and $J(O^1D)$, resulting in an O_3 formation rate ($F(O_3)$) comparable to that in spring. On the other hand, the O_3 destruction rate ($D(O_3)$) was much lower than that in spring because of the lowest values of $J(O^1D)$, H_2O, OH, and HO_2. The combination of these factors resulted in the highest net O_3 formation rate ($P(O_3)$) in January. This balance tends to shift as the season progresses. In March, calmer winds, combined with higher OH, reduce the NO concentrations. The increases in HO_2 and other peroxy radicals compensate for the NO reduction and maintain $F(O_3)$ essentially unchanged. However, the destruction rate is 2 times higher because of higher $J(O^1D)$, H_2O, OH, HO_2, and O_3, resulting in a 25% reduction in $P(O_3)$ from January. In April–May, both $F(O_3)$ and $D(O_3)$ become highest because of the highest photochemical activity, but $P(O_3)$ is lowest (negative), as the two largest terms become closer in value. The $P(O_3)$ in the boundary layer made a major contribution to the column-integrated $P(O_3)$, especially in winter.

[44] In the middle troposphere, $P(O_3)$ was lowest because of the lowest NO and moderately low H_2O concentrations. This holds also in September (PEM-W-A period). O_3 was closest to photochemical steady state in this altitude region, where O_3 lifetime is 100–200 days in winter. Moderately long transport times from fresh NO emissions, located below and above, should lower the NO levels and allow O_3 to be closer to the steady state values, despite the long O_3 lifetimes.

[45] In the upper troposphere (6–12 km), $P(O_3)$ was positive throughout the period from January to May. The net O_3 formation in this region constituted about 14–60% of the column-integrated O_3 formation. This net O_3 formation was observed also in September 1991 and February–March 1994, indicating that O_3 is stably produced in the upper troposphere throughout most of the year. This net O_3 formation is due to the NO levels greatly exceeding the critical level. The small number of data points obtained in the upper troposphere prevents the use of statistical analysis to quantify contributions of different sources of NO_x in the upper troposphere.

[46] At 20°–30°N, the seasonal transition of ozone chemistry in the boundary layer from winter to spring was qualitatively the same as that at 30°–45°N. However, quantitatively, NO was lower and $J(O^1D)$, H_2O, OH, and HO_2 were higher than at 30°–45°N in January and March. A higher fraction of NO_x emitted from the Asian continent was oxidized before reaching this region because of the higher OH and weaker outflow from the Asian continent, leading to the 3-times-lower NO levels in January at 20°–30°N than at 30°–45°N. $F(O_3)$ in January at 20°–30°N was 25% larger than that at 30°–45°N, compensated by the 2-to-3-times-higher HO_2. In March, $P(O_3)$ turned negative, indicating that it changes sign about one month earlier than it does at 30°–45°N, because of lower $F(O_3)$ (lower NO) and higher $D(O_3)$.

[47] Integrated $F(O_3)$ values are 4–9 times larger than the estimated O_3 influx from the stratosphere during January–April/May. It is also estimated that dry deposition of O_3 should have only a small influence on the integrated $P(O_3)$ during this period.

[48] The seasonal variation shown here should be interpreted as representing that in the region close to anthropogenic sources of NO_x, where NO_x concentrations are still high. Similar seasonal variation of $P(O_3)$ can prevail downwind of other continental sources, because the parameters $J(O^1D)$, H_2O, OH, HO_2, and wind fields, which control $P(O_3)$, are considered to follow similar seasonal variations. In this regard, there can be other regions where seasonal variations of the O_3 chemistry can be interpreted in a similar way.

[49] Comparison of the present western Pacific data with those obtained at 40°–60°N over North America shows differences in the seasonal variation in O_3 photochemistry. Much lower NO_x led to much lower $P(O_3)$ in the boundary layer over North America in winter and early spring, demonstrating the importance of high NO_x in the higher O_3 production rates over the western Pacific.

[50] **Acknowledgments.** We are indebted to all of the PEACE-A and B participants for their cooperation and support. Special thanks are due to the flight and ground crews of the G-II aircraft of Mitsubishi Diamond Air Service Co. Calibration of the filter radiometers was made by R. L. McKenzie of NIWA. We thank N. Toriyama and M. Kanada for their technical assistance with the measurements of reactive nitrogen. The meteorological data were supplied by the European Centre for Medium-Range Weather Forecasts (ECMWF). This work was supported in part by the Ministry of Education, Culture, Sports, Science, and Technology (MEXT).

References

Akimoto, H. (2003), Global air quality and pollution, *Science*, *302*, 1716–1719.

Atlas, E. L., B. A. Ridley, and C. A. Cantrell (2003), The Tropospheric Ozone Production about the Spring Equinox (TOPSE) Experiment: Introduction, *J. Geophys. Res.*, *108*(D20), 8353, doi:10.1029/2002JD003172.

Bais, A. F., et al. (2001), SUSPEN intercomparison of ultraviolet spectroradiometers, *J. Geophys. Res.*, *106*, 12,509–12,525.

Browell, E. V., et al. (2003), Large-scale ozone and aerosol distributions, air mass characteristics, and ozone fluxes over the western Pacific Ocean in late winter/early spring, *J. Geophys. Res.*, *108*(D20), 8805, doi:10.1029/2002JD003290.

Cantrell, C. A., J. G. Calvert, A. Bais, R. E. Shetter, B. L. Lefer, and G. D. Edwards (2003a), Overview and conclusions of the International Photolysis Frequency Measurement and Modeling Intercomparison (IPMMI) study, *J. Geophys. Res.*, *108*(D16), 8542, doi:10.1029/2002JD002962.

Cantrell, C. A., et al. (2003b), Steady state free radical budgets and ozone photochemistry during TOPSE, *J. Geophys. Res.*, *108*(D4), 8361, doi:10.1029/2002JD002198.

Crawford, J. H., et al. (1997), An assessment of ozone photochemistry in the extratropical western North Pacific: Impact of continental outflow during the late winter/early spring, *J. Geophys. Res.*, *102*, 28,469–28,487.

Davis, D. D., et al. (1996), Assessment of ozone photochemistry tendency in the western North Pacific as inferred from PEM-West A observations during the fall 1991, *J. Geophys. Res.*, *101*, 2111–2134.

Davis, D. D., et al. (2003), An assessment of western North Pacific ozone photochemistry based on springtime observations from NASA's PEM-West B (1994) and TRACE-P (2001) field studies, *J. Geophys. Res.*, *108*(D21), 8829, doi:10.1029/2002JD003232.

Emmons, L., et al. (2003), Budget of tropospheric ozone during TOPSE from two chemical transport models, *J. Geophys. Res.*, *108*(D8), 8372, doi:10.1029/2002JD002665.

Fuelberg, H. E., C. M. Kiley, J. R. Hannan, D. J. Westberg, M. A. Avery, and R. E. Newell (2003), Meteorological conditions and transport pathways during the Transport and Chemical Evolution over the Pacific (TRACE-P) experiment, *J. Geophys. Res.*, *108*(D20), 8782, doi:10.1029/2002JD003092.

Jacob, D. J., et al. (2003), Transport and Chemical Evolution over the Pacific (TRACE-P) aircraft mission: Design, execution, and first results, *J. Geophys. Res.*, *108*(D20), 9000, doi:10.1029/2002JD003276.

Kawa, S. R., and R. Pearson Jr. (1989), Ozone budgets from the dynamics and chemistry of marine stratocumulus experiment, *J. Geophys. Res.*, *94*, 9809–9817.

Koike, M., et al. (1997), Reactive nitrogen and its correlation with O_3 and CO over the Pacific in winter and early spring, *J. Geophys. Res.*, *102*, 28,385–28,404.

Kondo, Y., et al. (1997), Profiles and partitioning of reactive nitrogen over the Pacific Ocean in winter and early spring, *J. Geophys. Res.*, *102*, 28,405–28,424.

Kondo, Y., et al. (1999), Impact of aircraft emissions on NOx in the lowermost stratosphere at northern midlatitudes, *Geophys. Res. Lett.*, *26*, 3065–3068.

Kondo, Y., M. Ko, M. Koike, S. Kawakami, and T. Ogawa (2002), Preface to special section on Biomass Burning and Lightning Experiment (BIBLE), *J. Geophys. Res.*, *107*, 8397, doi:10.1029/2002JD002401. [printed *108*(D3), 2003]

Lamarque, J.-F., G. P. Brasseur, P. G. Hess, and J.-F. Müller (1996), Three dimensional study of the relative contributions of the different nitrogen sources in the troposphere, *J. Geophys. Res.*, *101*, 22,955–22,968.

Lenschow, D. H., R. Pearson Jr., and B. B. Stankor (1982), Measurements of ozone vertical flux to ocean and forest, *J. Geophys. Res.*, *87*, 8833–8837.

Levy, H., II, W. J. Moxim, K. A. Klonecki, and P. S. Kashibhatla (1999), Simulated tropospheric NO_x: Its evaluation, global distribution and individual source contributions, *J. Geophys. Res.*, *104*, 26,279–26,306.

Logan, J. A. (1985), Tropospheric ozone: Seasonal behavior, trends, and anthropogenic influence, *J. Geophys. Res.*, *90*, 10,463–10,482.

Logan, J. A. (1999), An analysis of ozonesonde data for the troposphere: Recommendations for testing 3-D models and development of a gridded climatology for tropospheric ozone, *J. Geophys. Res.*, *104*, 16,115–16,149.

Logan, J. A., M. J. Prather, S. C. Wofsy, and M. B. McElroy (1981), Tropospheric chemistry: A global perspective, *J. Geophys. Res.*, *86*, 7210–7254.

McKenzie, R., P. Johnston, A. Hofzumahaus, A. Kraus, S. Madronich, C. Cantrell, J. Calvert, and R. Shetter (2002), Relationship between photolysis frequencies derived from spectroscopic measurements of actinic fluxes and irradiances during the IPMMI campaign, *J. Geophys. Res.*, *107*(D5), 4042, doi:10.1029/2001JD000601.

McKenzie, R., D. Smale, M. Kotkamp, P. Johnston, and B. Liley (2003), Report on calibration of actinic flux photometers, *Rep. LAU2003-001*, Natl. Inst. of Water and Atmos. Res., Lauder, New Zealand.

Miyazaki, Y., K. Kita, Y. Kondo, M. Koike, M. Ko, W. Hu, S. Kawakami, D. R. Blake, and T. Ogawa (2002), Springtime photochemical ozone production observed in the upper troposphere over east Asia, *J. Geophys. Res.*, *107*, 8398, doi:10.1029/2001JD000811. [printed *108*(D3), 2003]

Miyazaki, Y., et al. (2003), Synoptic-scale transport of reactive nitrogen over the western Pacific in spring, *J. Geophys. Res.*, *108*(D20), 8788, doi:10.1029/2002JD003248.

Nakamura, K., et al. (2003), Measurement of NO_2 by photolysis conversion technique during TRACE-P, *J. Geophys. Res.*, *108*(D24), 4752, doi:10.1029/2003JD003712.

Olson, J. R., et al. (2004), Testing fast photochemical theory during TRACE-P based on measurements of OH, HO_2, and CH_2O, *J. Geophys. Res.*, *109*, D15S10, doi:10.1029/2003JD004278.

Oshima, N., et al. (2004), Asian chemical outflow to the Pacific in late spring observed during the PEACE-B aircraft mission, *J. Geophys. Res.*, *109*, D23S05, doi:10.1029/2004JD004976, in press.

Parrish, D. D., Y. Kondo, O. R. Cooper, C. A. Brock, D. A. Jaffe, M. Trainer, T. Ogawa, G. Hübler, and F. C. Fehsenfeld (2004), Intercontinental Transport and Chemical Transformation 2002 (ITCT 2K2) and Pacific Exploration of Asian Continental Emission (PEACE) experiments: An overview of the 2002 winter and spring intensives, *J. Geophys. Res.*, *109*, D23S01, doi:10.1029/2004JD004980, in press.

Singh, H. B., Y. Chen, G. L. Gregory, G. W. Sachse, R. Talbot, D. R. Blake, Y. Kondo, J. D. Bradshaw, B. Heikes, and D. Thornton (1997), Trace chemical measurements from the northern mid-latitude lowermost stratosphere in early spring: Distributions, correlations, and fate, *Geophys. Res. Lett.*, *24*, 127–130.

Streets, D. G., et al. (2003), An inventory of gaseous and primary aerosol emissions in Asia in the year 2000, *J. Geophys. Res.*, *108*(D21), 8809, doi:10.1029/2002JD003093.

Stroud, C., et al. (2004), Photochemistry in the Arctic free troposphere: Ozone budget and its dependence on nitrogen oxides and the production rate of free radical, *J. Atmos. Chem.*, *47*, 107–138.

Takegawa, N., et al. (2004), Removal of NO_x and NO_y in Asian outflow plumes: Aircraft measurements over the western Pacific in January 2002, *J. Geophys. Res.*, *109*, D23S04, doi:10.1029/2004JD004866, in press.

Thompson, A. M. (1992), The oxidizing capacity of the Earth's atmosphere: Probable past and future changes, *Science*, *256*, 1157–1165.

Tie, X., et al. (2003), Effects of sulfate aerosol on tropospheric NO_x and ozone budgets: Model simulations and TOPSE evidence, *J. Geophys. Res.*, *108*(D4), 8364, doi:10.1029/2001JD001508.

Wang, Y. J., J. A. Logan, and D. J. Jacob (1998a), Global simulation of tropospheric O_3-NO_x-hydrocarbon chemistry: 2. Model evaluation and global ozone budget, *J. Geophys. Res.*, *103*, 10,727–10,755.

Wang, Y. J., D. J. Jacob, and J. A. Logan (1998b), Global simulation of tropospheric O_3-NO_x-hydrocarbon chemistry: 3. Origin of tropospheric ozone and effects of nonmethane hydrocarbons, *J. Geophys. Res.*, *103*, 10,757–10,767.

Wang, Y., et al. (2003), Springtime photochemistry at northern mid and high latitudes, *J. Geophys. Res.*, *108*(D4), 8358, doi:10.1029/2002JD002227.

Wild, O., J. K. Sundet, M. J. Prather, I. S. A. Isaksen, H. Akimoto, E. V. Browell, and S. J. Oltmans (2003), Chemical transport model ozone simulations for spring 2001 over the western Pacific: Comparisons with TRACE-P lidar, ozonesondes, and Total Ozone Mapping Spectrometer columns, *J. Geophys. Res.*, *108*(D21), 8826, doi:10.1029/2002JD003283.

World Meteorological Organization (1999), Scientific assessment of ozone depletion: 1998, *Rep. 44*, Global Ozone Res. and Monit. Proj., Geneva.

Yienger, J. J., A. A. Klonecki, H. Levy, W. J. Moxim, and G. R. Carmichael (1999), An evaluation of chemistry's role in the winter-spring ozone maximum found in the northern midlatitude free troposphere, *J. Geophys. Res.*, *104*, 3655–3688.

D. R. Blake, Department of Chemistry, University of California, Irvine, Irvine, CA 92697-2025, USA. (drblake@uci.edu)

G. Chen, J. Crawford, and M. Ko, NASA Langley Research Center, Hampton, VA 23681, USA. (g.chen@larc.nasa.gov; j.h.crawford@larc.nasa.gov; malcolm.k.ko@larc.nasa.gov)

S. Kawakami, T. Ogawa, and T. Shirai, Earth Observation Research and Application Center, Japan Aerospace Exploration Agency, Harumi Island Triton Square Office Tower X 23F, 1-8-10, Harumi, Chuo-ku, Tokyo 104-6023, Japan. (kawakami.shuji@jaxa.jp; togawa@eorc.jaxa.jp; shirai@eorc.jaxa.jp)

K. Kita, Department of Environmental Science, Ibaraki University, Bunkyo 2-1-1, Mito, Ibaraki 310-8512, Japan. (kita@env.sci.ibaraki.ac.jp)

M. Koike, Department of Earth and Planetary Science, Graduate School of Science, University of Tokyo, 7-3-1 Hongo, Bunkyo-ku, Tokyo 113-0033, Japan. (koike@eps.s.u-tokyo.ac.jp)

Y. Kondo, Y. Miyazaki, K. Nakamura, and N. Takegawa, Research Center for Advanced Science and Technology, University of Tokyo, 4-6-1 Komaba, Meguro-ku, Tokyo 153-8904, Japan. (kondo@atmos.rcast.u-tokyo.ac.jp; yuzom@atmos.rcast.u-tokyo.ac.jp; nakamura@atmos.rcast.u-tokyo.ac.jp; takegawa@atmos.rcast.u-tokyo.ac.jp)

B. Liley, National Institute of Water and Atmospheric Research, Lauder, PB 50061 Omakau, Central Otago 9182, New Zealand. (b.liley@niwa.co.nz)

Y. Wang, School of Earth and Atmospheric Sciences, Georgia Institute of Technology, 221 Bobby Dodd Way, Atlanta, GA 30332-0340, USA. (ywang@eas.gatech.edu)